



Influence of composition of nuclear waste glasses on vapor phase hydration

Sathya Narayanasamy, Patrick Jollivet, Nicole Godon, Frédéric Angeli, S. Gin, Martiane Cabié, Julien Cambedouzou, Corentin Le Guillou, Abdesselam Abdelouas

► To cite this version:

Sathya Narayanasamy, Patrick Jollivet, Nicole Godon, Frédéric Angeli, S. Gin, et al.. Influence of composition of nuclear waste glasses on vapor phase hydration. Journal of Nuclear Materials, 2019, Journal of Nuclear Materials, pp.53-71. 10.1016/j.jnucmat.2019.07.015 . hal-02277978

HAL Id: hal-02277978

<https://hal.univ-lille.fr/hal-02277978>

Submitted on 27 Sep 2019

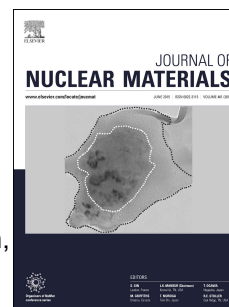
HAL is a multi-disciplinary open access archive for the deposit and dissemination of scientific research documents, whether they are published or not. The documents may come from teaching and research institutions in France or abroad, or from public or private research centers.

L'archive ouverte pluridisciplinaire **HAL**, est destinée au dépôt et à la diffusion de documents scientifiques de niveau recherche, publiés ou non, émanant des établissements d'enseignement et de recherche français ou étrangers, des laboratoires publics ou privés.

Accepted Manuscript

Influence of composition of nuclear waste glasses on vapor phase hydration

Sathya Narayanasamy, Patrick Jollivet, Nicole Godon, Frédéric Angeli, Stéphane Gin, Martiane Cabié, Julien Cambedouzou, Corentin Le Guillou, Abdesselam Abdelouas



PII: S0022-3115(19)30397-6

DOI: <https://doi.org/10.1016/j.jnucmat.2019.07.015>

Reference: NUMA 51715

To appear in: *Journal of Nuclear Materials*

Received Date: 1 April 2019

Revised Date: 12 July 2019

Accepted Date: 14 July 2019

Please cite this article as: S. Narayanasamy, P. Jollivet, N. Godon, Fr  . Angeli, St  . Gin, M. Cabi  , J. Cambedouzou, C. Le Guillou, A. Abdelouas, Influence of composition of nuclear waste glasses on vapor phase hydration, *Journal of Nuclear Materials* (2019), doi: <https://doi.org/10.1016/j.jnucmat.2019.07.015>.

This is a PDF file of an unedited manuscript that has been accepted for publication. As a service to our customers we are providing this early version of the manuscript. The manuscript will undergo copyediting, typesetting, and review of the resulting proof before it is published in its final form. Please note that during the production process errors may be discovered which could affect the content, and all legal disclaimers that apply to the journal pertain.

Influence of composition of nuclear waste glasses on vapor phase hydration

Sathya Narayanasamy^a, Patrick Jollivet^a, Nicole Godon^a, Frédéric Angeli^a, Stéphane Gin^a, Martiane Cabié^b, Julien Cambedouzou^{c,d}, Corentin Le Guillou^e, Abdesselam Abdelouas^f

^a CEA Marcoule, DEN, MAR, DE2D, SEVT/LCLT, bât 208, BP17171, 30207 Bagnols sur Cèze cedex, France

^b Aix Marseille Univ, CNRS, Centrale Marseille, FSCM, CP2M, Marseille France

^c ICSM, CEA, CNRS, ENSCM, Univ. Montpellier, Marcoule, France

^d IEM, CNRS, ENSCM, Univ. Montpellier, Montpellier, France

^e UMET-Unité Matériaux et Transformations, CNRS UMR 8207, Université de Lille, 59655 Villeneuve d'Ascq, France

^f SUBATECH, CNRS-IN2P3, IMT Atlantique-Université de Nantes, 4 rue Alfred Kastler, BP 20722, 44307 Nantes cedex 03, France

Abstract

For the first time, the influence of glass composition on the vapor hydration kinetics of the French AVM nuclear waste glass simulants was investigated. Three complex borosilicate glasses (> 20 oxides) along with three simplified Na/(Ca, Na)/(Mg, Na)-alumino-borosilicate glasses with four or five oxides were altered at 50°C in water vapor (95% RH) for up to 557 days. The solid characterization of the altered samples (by SEM, TEM, XRD, ToF-SIMS, SAXS) revealed that the rate-controlling vapor hydration mechanism is composition dependent. The vapor hydration rate of the more durable glasses, whose molar ratio of $\text{Al}_2\text{O}_3/(\text{CaO or MgO})$ is ≥ 1 , seems to be limited by network-hydrolysis, whereas the overall glass alteration rate of the less durable glasses, whose $\text{Al}_2\text{O}_3/\text{MgO}$ ratio is < 1 , seems to be driven by the precipitation of Mg-rich secondary phases. All the vapor hydrated glasses show the presence of a homogeneous gel layer of a few tens of nm thickness. The more durable glasses have a smaller quantity of secondary phases precipitated on their surface. The less durable glasses have a relatively significant quantity of secondary phases precipitated above the gel layer and irregularly shaped, scattered and highly porous altered zones formed beneath the gel layer. The overall alteration rate of the less durable glasses was 10-20 times faster than the more durable glasses. For all glasses, FTIR spectroscopy indicated an inflexion in the vapor hydration rate after 120-200 days of alteration, likely due to a passivating effect of the altered layer formed under unsaturated conditions. The average pore size of the altered layer in

certain vapor hydrated glasses measured by SAXS is similar to the pore sizes of the gel layer formed in aqueous medium and varies very slightly with glass composition.

1. Introduction

The high-level activity radioactive waste (HLW), issued from the nuclear power industry, is immobilized in a vitreous matrix, since glass has been proven to be a stable solid form for thousands of years based on archeological or geological evidence [1, 2]. According to the permanent nuclear waste disposal solution envisaged by ANDRA (the French national radioactive waste management agency), the waste glass packages (glass in a stainless steel canister encased in a low-alloy steel overpack) will be stored in an underground repository constructed with steel and concrete reinforcements in clay layer 500 m beneath the earth's surface. The steel corrosion in the closed underground repository would result in hydrogen gas liberation. As a result, the re-saturation of the site with ground water from the surrounding clay medium will be slowed down. Consequently, it is expected that nuclear waste glasses maybe exposed to an unsaturated medium for up to tens of thousands of years before being completely immersed in aqueous ground water [3]. Therefore it is mandatory to investigate the consequences of glass alteration in vapor phase, the mechanisms involved and the influence of intrinsic and extrinsic parameters [4]. Glass alteration in vapor phase has been relatively less studied in comparison to alteration in aqueous medium [5-15].

Vapor hydration experiments on a variety of nuclear waste glasses and their non-radioactive surrogates have been conducted by different laboratories in USA [16-26], UK [27] and France [28-33]. From the experimental results so far, it can be understood that the reactions occurring between glass and water are the same for alteration in aqueous medium and unsaturated water vapor. However, the rate controlling reaction mechanism and the driving force for alteration are different in both cases. The difference arises largely due to the very small volume of water in vapor phase and almost no leaching by solution, unless water condenses and flows away from the altered surface. The precipitation of secondary phases seems to be the strongest driving force for alteration in vapor phase at high temperature. A majority of the vapor hydration studies conducted so far have been done in extreme conditions (150-200°C & 100% relative humidity (RH)) favorable for secondary phases precipitation. This temperature range is not representative of the expected scenario in the French geological disposal facility. It is expected that the temperature of the waste glass packages will be lower than or equal to 50°C [34]. The vapor hydration of SON68 (French inactive reference nuclear waste glass) at high temperatures (90-200°C, activation energy (E_a)=43-47 KJ/mol) [28] and lower temperatures (35-90°C,

$E_a=34\pm0.4$ KJ/mol) [31] suggests that the rate-controlling mechanisms may depend on temperature. The limited data of the studies have also confirmed the influence of relative humidity [16], glass composition [22, 27, 35-37], composition of the vapor phase [30] and radioactivity [38] on vapor hydration kinetics. Insights on glass alteration in vapor phase can also be obtained from studies on atmospheric alteration of window glasses, art crafts, stained-glass windows of historic sites etc. [39-41]. Almost all these studies have shown similar altered layer morphology on the glass surface in contact with an unsaturated medium. An altered layer, commonly referred to as 'gel layer', is formed adjacent to pristine glass. This gel layer has been suggested to be formed by mechanisms of hydration (penetration of water molecules) [37] / inter-diffusion ($(\equiv Si - O^-M^+)_{glass} + H_{water}^+ \rightarrow (\equiv Si - OH)_{glass} + M_{water}^+$) [40, 42] / network hydrolysis ($(\equiv Si - O - Si \equiv)_{glass} + H_2O \rightarrow 2 (\equiv Si - OH)_{glass}$) [31, 43, 44] or a combination of these mechanisms [39, 41]. Localized dissolution-precipitation or condensation mechanisms and re-organization of the gel layer have also been discussed in literature [31, 39]. On the surface of this gel layer, amorphous / crystalline secondary precipitates maybe present [23, 31, 36]. In certain cases, the secondary phases may also accelerate the vapor hydration kinetics [22].

In this article, the focus is on the influence of glass composition on vapor hydration. Through literature survey, it can be understood that glass composition can affect glass durability in three ways. (i) The presence of alkaline elements in the glass can promote the quantity of water adsorbed on surface, facilitate inter-diffusion mechanism and may result in increased hydration rate [22, 37, 45]. (ii) Glass composition plays an important role in the precipitation of secondary phases under given conditions and thus may accelerate glass alteration [22, 35]. (iii) Presence of elements such as Zn, which increases the resistance to network hydrolysis, may increase glass durability in vapor phase [27]. The literature study led us to understand that certain elements such as Al may have a dual role depending on whether the conditions are favorable for secondary phase precipitation (negative effect) or if they participate in increasing the resistance of glass network to hydrolysis (positive effect). Therefore, the temperature of the experiments needs to be carefully chosen, as the influence of the glass composition on its alteration could vary with temperature.

In this study, the influence of nuclear waste glass composition on vapor hydration has been investigated by studying the behavior of three AVM (*Atelier de Vitrification de Marcoule*) glasses in contact with water vapor. The AVM glasses are complex borosilicate glasses containing more than 20 oxides including fission products issued from the UNGG (*Uranium Naturel Graphite-Gaz*) reactor at Marcoule. The range in the AVM glasses composition is extensive due to the variation in the composition of fission products

solution. The long-term behavior of these HLW radioactive glasses in aqueous media was studied using many inactive surrogates [46, 47]. Based on this study, the glasses AVM6, AVM10 and AVMV4 are the three inactive surrogates selected for the current study. AVM6 is known to alter at the highest residual rate (r_r) in deionized water at 50°C and AVM10 alters at the lowest r_r . AVMV4 is a simulant of the actual composition of the HLW glass produced at Marcoule facility.

The specific influence of alkaline-earth elements such as Mg and Ca was investigated, since AVM glasses contain a significant amount of Mg and very little Ca and the effects of these elements on glass alteration rate in aqueous medium are relatively well-known [48-52]. Based on literature review, it is expected that these elements would be detrimental to glass durability in unsaturated medium due to their tendency to form secondary precipitates. The study of their specific influence cannot be carried out using a complex glass with several oxides due to possible interference and synergies between other elements. Therefore, three simplified glasses (Q, QCa and QMg) were prepared based on the Si/Al stoichiometry of AVMV4. The use of simplified glass compositions helps to understand the role of specific element on glass durability [53-56].

The fission products loading of AVM glasses suggests that the temperature of the glass packages during the expected time of exposure to water vapor will be around 50°C. Therefore, it was decided to conduct our experiments at 50°C. It is suspected that the rate-controlling vapor hydration mechanisms may vary with conditions favorable for precipitations of certain silica-rich secondary phases at higher temperatures (>90°C). The relative humidity (RH) was chosen to be 95% since the conditions expected in the repository are close to saturation [34].

2. Materials and methods

2.1 Sample preparation

The synthesis of the AVM glasses has already been described by Thien [46]. The glass samples for this study were retrieved from the same batch. Q, QCa and QMg were prepared using the oxide precursors (SiO_2 , H_3BO_3 , Na_2CO_3 , Al_2O_3 , CaO (for QCa) and MgO (for QMg)). The mixtures were put in a Pt-Rh crucible and heated during 3 h at 1450°C. They were then annealed at 620°C during 1 h in a graphite crucible. Afterwards, the temperature of the furnace was decreased at a rate of 0.5°C/min until 300°C and then it was turned off. The compositions of the glasses after dissolution in acid solution were determined by Inductively Coupled Plasma-Optical Emission Spectroscopy (ICP-OES). The data in mol% oxides are provided in table 1. The error percentage associated with the measured values is 3%. The

fraction of Non-Bridging Oxygen (NBO) atoms in the glass network was theoretically calculated based on equation 2.1.1 and equation 2.1.2. ^{11}B NMR spectra (not presented here) were collected on a Bruker Avance II 500WB spectrometer. The calculated NBO values and the fraction of $\text{B}^{(\text{IV})}$ for each glass are provided in table 1. The error associated varies between 3 to 8%.

$$NBO = \frac{2 * (\text{mol fr. of oxides of modifier cations} - \text{mol fr. of oxides of network former requiring charge compensation})}{N(O)} \quad \text{Equation 2.1.1}$$

$$N(O) = \sum (\text{no. of oxygen atoms in 1 molecule of oxide} * \text{mol fr. of oxide}) \quad \text{Equation 2.1.2}$$

For all glasses, the NBO values are similar despite their differences in compositions (except Q). The percentage of $\text{B}^{(\text{IV})}$ in each glass shows that Mg is less efficient to compensate $[\text{BO}_4]^-$ entities than Ca.

For each glass, two monoliths of dimensions ($2.5 \times 2.5 \times 0.1 \text{ cm}^3$) were prepared for vapor hydration during 180 days and 557 days, respectively. These monoliths were cut from the glass bars and polished to optical finish (surface roughness $< 1 \mu\text{m}$) on both faces. Similarly, one polished monolith for each glass was also prepared with dimensions ($2.5 \times 2.5 \times 0.08 \text{ cm}^3$) for the purpose of studying hydration kinetics using Fourier Transform Infrared (FTIR) spectroscopy. All the glass monoliths were washed in ultra-pure acetone and absolute ethanol under ultrasonic agitation and dried for a few hours in an oven at 50°C before starting the experiment. Powder samples of each glass were prepared by crushing glass pieces using Retsch MM400 ball-mill apparatus equipped with tungsten carbide balls. The size fraction of $2 - 5 \mu\text{m}$ were separated using pure acetone solvent and the application of Stokes law, for Small Angle X-ray Scattering (SAXS) measurement.

2.2 Alteration Protocol

A WEISS WKL64 climatic chamber was used to hydrate the samples at 50°C and 95% RH. The apparatus continuously monitors and displays the temperature and RH in the test zone. De-mineralized water is used to produce steam and then de-humidified to have the programmed RH in the test zone. The monolithic glass samples are placed horizontally in a curved grid Teflon basket that allows the sample to be exposed to vapor on both faces. The glass powders were dispersed in plastic petri dishes. Similar protocol for vapor hydration of glasses has been used before in literature [39].

2.3 Experiments

2.3.1 Hydration kinetics

A glass monolith of dimensions ($2.5 \times 2.5 \times 0.08 \text{ cm}^3$) was placed in the climatic chamber at 50°C and 95% RH. The sample was removed periodically (approximately once a month) for a short duration (~ 10 minutes) and analyzed in transmission mode using a Vertex 70 FTIR spectrometer. It was then replaced in the chamber to continue hydration. Five spectra at different regions of the monolith were recorded and averaged. The diameter of the diaphragm was set to 6 mm. The spectra were recorded from 4000 to 400 cm^{-1} . The deconvolution of the spectra from 4000 to 2600 cm^{-1} into five Gaussian bands was attributed to the vibration of the OH stretching mode in SiOH molecules ($\sim 3595\text{-}3605 \text{ cm}^{-1}$), bound water-silanol groups ($\sim 3515\text{-}3518 \text{ cm}^{-1}$ & $\sim 3170\text{-}3185 \text{ cm}^{-1}$), symmetrical OH stretching mode in the free water molecule ($\sim 3400\text{-}3415 \text{ cm}^{-1}$) and the glass matrix ($\sim 2700 \text{ cm}^{-1}$). This type of deconvolution is based on the protocol used to follow vapor hydration kinetics using infrared spectroscopy in recent literature [29, 32, 57, 58]. The hydration kinetics was followed by studying the evolution of the increase in absorbance of the band attributed to the OH stretching mode in SiOH molecules over time.

Calculation of error in the increase in absorbance values: With every deconvolution, the standard error associated with the increase in the area of the Gaussian is calculated by Origin software. The error values for the Gaussian fit are less than 2%. However, while measuring the FTIR spectrum at 5 different places for the same sample, the sample compartment is opened and closed. Due to this the background that was earlier measured is disturbed. Therefore, several backgrounds were measured throughout the day of the FTIR analysis, and the standard deviation among the absorbance values in the range of wavenumbers $3595\text{-}3605 \text{ cm}^{-1}$ was used to calculate the error value. After error propagation calculation, 0.02 (a.u.) was calculated as the error value.

2.3.2 Characterization of altered glasses

For each composition, two glass monoliths of dimensions ($2.5 \times 2.5 \times 0.1 \text{ cm}^3$) and the glass powders were placed in the climatic chamber at 50°C and 95% RH for a period of 180 days and 557 days respectively. Afterwards, the monoliths were removed from the chamber and cut into dimensions of ($1 \times 1 \times 0.1 \text{ cm}^3$) approximately for characterization by Scanning Electron Microscope (SEM), Transmission Electron Microscope (TEM), X-Ray Diffraction (XRD) and Time-of-Flight Secondary Ion Mass Spectrometry (ToF-SIMS). The glass powders were characterized by Small Angle X-ray Scattering (SAXS) to probe the porosity and the pore-size of the gel layer.

For the purpose of studying the evolution of pore characteristics of the gel layer with time, the powdered samples of AVM6 were altered for 11 days, 31 days and 90 days at 50°C and 95% RH, in addition to the standard alteration time of 180 days and 557 days. These samples were characterized by SAXS.

2.4 Characterization techniques

2.4.1 SEM

Morphological analysis of the altered samples were carried out using a field emission Scanning Electron Microscope (SEM) Zeiss Gemini Supra 55, JEOL JSM 6330F with an Energy Dispersive Spectroscopy (EDS) system.

2.4.2 TEM

FEI TECNAI G2 Transmission Electron Microscope (TEM) was used for morphological and chemical analysis. The 80 kV to 200 kV TEM permits to do conventional imaging and analytics, disposes of bright-field and dark-field imaging, EDS and Scanning TEM (STEM) to probe chemical composition of materials. The spatial resolution is 0.27 nm. Ultra-thin samples for observation by TEM (the length of the sample is approx. 5 μm and it is about one hundred nm thick) were prepared using Dual Beam FIB (FEI Helios 600 NanoLab). The uncertainty associated with the quantitative STEM-EDX analyses was estimated to be around 12% relative error. Scanning transmission electron microscopy (STEM) and EDS mapping were performed on QMg sample altered for 180 days using a Thermofisher Titan Themis 300 microscope operated at 300 keV, located at the "Centre Commun de Microscopie – CCM" at the university of Lille. Hyperspectral EDS data were obtained using the super-X detector system equipped with four windowless silicon drift detectors. The probe current was set at 50 pA. The analysis of the hyperspectral data was performed using the Hyperspy python-based package [59]. The signal was first denoised using Principal Component Analysis (PCA). Then, the EDS spectra at each pixel were fitted by a series of Gaussian functions and a physical model for background/bremsstrahlung. Quantification was performed thanks to the Cliff-Lorimer method, using experimentally determined k-factors and absorption correction routines.

2.4.3 XRD

Crystalline secondary phases were identified using a Philips X'Pert diffractometer X-Ray Diffraction (XRD) apparatus equipped with a copper tube and a goniometer (4-80° 2 θ , step size 0.01744°). Each glass monolith was analyzed for 12 h on a multiple purpose sample stage (MPSS).

2.4.4 ToF-SIMS

The behavior of elements in the altered layer was characterized using ToF-SIMS (SSIMS on TOF 5 (IONTOF)). Depth profiles of secondary positive ions were obtained by alternating analysis and abrasion cycles. 25 keV Bi_1^+ primary ions at 2 pA current were used for analysis cycles. 1 keV primary O_2^+ ions at 250 nA current were used for the abrasion cycles. The eroded area was $200 \times 200 \mu\text{m}^2$. The analyzed area was $60 \times 60 \mu\text{m}^2$ for the samples altered for 180 days and $50 \times 50 \mu\text{m}^2$ for the samples altered for 557 days. The surface charge was neutralized on the monoliths by a pulsed low-energy (<20 keV) electron flux. The depth calibration was carried out using the abrasion rate and a mechanical profilometer to measure the crater depth at the end of the analysis. It is to be noted that the same abrasion rate was used for analyzing the gel layer and the pristine glass. This choice was justified by the good correspondence between thickness of altered layer measured by SEM and ToF-SIMS in other works [31].

The profiles were normalized with respect to the intensity of each element (C) in the pristine glass (denoted as PG) and with respect to the intensity of Si (C_{Si}) at given depth as shown in the equation 2.4.4.1 below.

$$\text{Normalized intensity} = \frac{\frac{C}{C_{\text{Si}}}}{\left(\frac{C}{C_{\text{Si}}}\right)_{\text{PG}}} \quad \text{Equation 2.4.4.1}$$

$$\text{Altered layer depth} = x_0 \text{ at which } \left(0.5 - \frac{\frac{C_B}{C_{\text{Si}}}}{\left(\frac{C_B}{C_{\text{Si}}}\right)_{\text{PG}}} = 0 \right) \quad \text{Equation 2.4.4.2}$$

In literature, the most immobile element in the glass network is used for normalization of ToF-SIMS profiles to avoid matrix effects, which could be either Si or Zr [60, 61]. In our experiments, Si can be considered immobile. This is valid after verification that Si bearing phases are in relatively small quantity. It was chosen as the element for normalization since it is present in a sufficiently large quantity in the glass, such that the precipitation of secondary phases on the glass surface will not result in depletion of a large fraction of this element.

Boron is a good tracer for glass alteration in aqueous medium since it is neither retained in the gel layer nor forms secondary phases. In vapor phase it would be logical to expect that the retention of boron in the gel layer is much higher since the quantity of water available to leach boron is highly limited. However, the ToF-SIMS profiles indicate that the retention of boron in the gel layers is very limited (< 20%). Therefore, boron is used as a tracer to measure altered layer thickness in the vapor hydration

phenomenon as well. The thickness of the altered layer was determined based on the profile of boron as shown in equation 2.4.4.2. The thickness of the zone of interface between gel layer and pristine glass measured by ToF-SIMS could be influenced by sample artefacts such as surface roughness of the sample due to precipitates or due to the heterogeneity of the altered layer.

2.4.5 SAXS

The apparatus used is a SAXS-Mo apparatus emitting monochromatic X-ray beam at λ 0.709 Å and the photon flux is 3×10^6 photons.s⁻¹ approximately. The q-range covered is 0.2 to 30 nm⁻¹. The distance scale D is related to the scattering vector q by the formula $D = 2\pi/q$. The sample was filled in a glass capillary tube of 2 mm (e_s) diameter and approximately 10 µm wall thickness. In the section of the sample analyzed, the inter-grain porosity is filled with air. The inner porosity of each grain could be filled with air or water. The data treatment for a porous or granular medium with special attention to the case of glass leaching by water was handled by Spalla et al. 2003 [62]. The data treatment was based on previous works [62-64] and is explained in detail in the supplementary data (section1).

3. Results

The solid characterization of the altered glass has given insights into the morphology of the altered layer, behavior of elements in the altered layer, porosity of the altered layer and the vapor hydration kinetics. In each subsection, the results of all six glasses have been presented. An overall analysis of the results showed that the behavior of the altered glasses AVM6 and AVM10 is similar and that of AVMV4 and QMg is similar. For this reason, the results of these two couples of glasses have been presented together in section 3.1 and section 3.3. The Q and QCa glasses, which do not contain Mg, are also presented following the four above mentioned Mg-containing glasses.

3.1 Morphology of the altered layer (SEM/TEM images)

3.1.1 AVM6 and AVM10

The SEM images showed that the alteration of these two glasses is similar in the following accounts:

(i) Irregular alteration: SEM images of cross-sections showed that both glasses had altered in a heterogeneous manner. Figure 1 shows the SEM and TEM cross-sections of AVM6 and AVM10 altered for 180 days and 557 days (denoted hereafter as AVM6-180, AVM6-557, AVM10-180 and AVM10-557).

The altered surface was punctuated with low density altered zones in the shape of irregular cups whose widths and depths varied from a few hundred nm to a few μm (figure 1 (a) and (c) and supplementary data-figure S 1). They were formed on both faces. TEM images of micro-sections showed that in both glasses, these irregular zones were highly porous. This was the case for all four samples. According to STEM-EDX analysis (supplementary data-Section 3, figures S 6, S 7 and S 8), the porous zone is depleted in Mg, Fe and enriched in Ca.

An attempt to calculate a statistical average thickness of the altered layer of the AVM10-180 sample was made. Ten cross-section SEM images on both faces of AVM10-180 were taken. These images spanned a width of approx. 10 μm each and were taken at a distance of approx. 500 μm apart from one another. From these images, 334 measurements of the irregular altered zone thicknesses were calculated using GIMP image processing software. The average of these measurements for the AVM10 glass is around 659 nm. The minimum thickness measured is 78 nm and the maximum thickness measured is 1.9 μm . The same process could not be repeated for other samples due to technical difficulties.

(ii) Precipitation of Mg-rich phyllosilicates and other secondary precipitates: Both glass surfaces were covered by secondary precipitates. SEM images showed well-developed leafy precipitates on both AVM6-180 and AVM6-557 (figure 2(a) and figure 1(b)). Needle shaped precipitates were present sporadically on the altered surface (figure 2(a)). In AVM6-557, these needle-shaped phases were much more developed and formed clusters. As shown in figure 2(c) and 2(d), curiously, these clusters formed in straight lines. It seems as though these phases preferentially formed along surface defects created during sample preparation (polishing). TEM images also showed the presence of a layer of phyllosilicates on the surface of the micro-sections that measured approx. 70 nm in AVM6-180 (Figure 2(b)) and approx. 200-250 nm in AVM6-557 (figure 1 (b)). TEM-EDX analysis and EDS mapping of an altered zone also indicated that the phyllosilicates were enriched in Mg, Fe and Na in addition to Si and they were depleted in Al with respect to the pristine glass composition (supplementary data –section 3, figure S 6 and S 7). Figure S4 in supplementary data shows the enrichment of Mg in the phyllosilicate layer.

The leafy precipitates in AVM10-180 seemed to be under-developed and visually different in comparison to AVM6. In AVM10-557, they were better developed than AVM10-180, as can be seen in figure 2(f) in comparison to 2(e). This can also be affirmed by the SEM & TEM images provided in the supplementary data-section 2, figure S 3. The quantity of the needle shaped crystalline phases also seem lower than that on the AVM6 samples and the AVM10-557 samples seem to contain more of them than

AVM10-180 samples (supplementary data- figure S 2). The TEM images show a phyllosilicate layer of approx. 300 nm thickness for AVM10-180 and approximately 70 nm thick phyllosilicate layer for AVM10-557 (figures 2(e) and 2(f)). It is to be noted here that it is not the overall layer thickness, but just the thickness of the phyllosilicate section.

(iii) The third similarity between AVM6 and AVM10 samples is the presence of a dense homogeneous gel layer beneath the phyllosilicate layer but above the porous irregularly altered zones. This gel layer is approximately 50 nm thick in AVM6-180 (figure 2(b)) and 70 nm thick in AVM6-557 (figure 1(b)). It is approx. 30 nm thick in AVM10-180 and AVM10-557 (figures 2(e) and 2(f) respectively). This layer is enriched in Mg, Si and Ca, and sometimes slightly depleted in Al (supplementary data- figures S 5, S 6, S 7 and S 9).

To summarize, under the tested conditions, AVM6 and AVM10 glasses alter similarly, which is not the case for aqueous alteration of these glasses at the same temperature. The altered surface is composed of a phyllosilicate layer at the top (few tens to a few hundreds of nm thick) that is composed of Si, Al, Mg, Fe, Ca and Na. Underneath the phyllosilicates, TEM images have revealed a uniform gel layer of a few tens of nm thickness that seems enriched in Mg and Si and depleted in Al, with respect to the pristine glass. Porous irregularly altered zones are present in a heterogeneous/discontinuous manner beneath the gel layer.

Identification of secondary precipitates

The compositions of the phyllosilicates were analyzed using STEM-EDX. It is to be noted that the Na concentration was not constant throughout the analysis. The Na atoms migrated under the beam towards the resin. It was verified that the concentration of other major elements were not affected due to long exposure to electron beam. The stoichiometry of elements (excluding Na) in the phyllosilicate layer, calculated from the STEM-EDX analysis, for the four samples described in section 3.1.1 are provided in table 2 (the estimated uncertainty is around 12% relative error). It can be noted that the composition of phyllosilicates is variable during the alteration of different glasses. No correlation could be identified with pristine glass compositions (Si/Al ratio for example) as was previously suggested [65]. The phyllosilicates formed on AVM6-180 and AVM6-557 have a very similar composition. The stoichiometric ratio of Si/Mg suggests that the composition of the phyllosilicates formed on AVM6 glass is similar to that of a di-octahedral smectite such as montmorillonite- $((\text{Na,Ca})_{0.33}(\text{Al,Fe,Mg})_2(\text{Si}_4\text{O}_{10})(\text{OH})_2 \cdot$

nH₂O), with slight variations in the composition based on the different transition metal substitutes available. The quantity of Al and other elements capable of occupying octahedral sites in the smectite (Mg, Fe) is not sufficient to envisage a tri-octahedral smectite.

The XRD patterns of the AVM6 samples showed an intense peak corresponding to (001) reflection at 15 Å (supplementary data figure S 10), which can be associated with montmorillonites [66]. Other peaks, if present, were not clearly distinguishable from the background noise. Apart from the composition given by EDX analyses, the other method to distinguish di-octahedral smectites from tri-octahedral smectites is the appearance of the (060) reflection between 1.49 and 1.51 Å [67, 68]. It is difficult to distinguish the peaks around 1.51 Å in the XRD patterns from the background noise. The physical magnitude represented by the (001) and (060) lines have different orientations. Therefore, it is possible that the intensity of one of the two peaks increases preferentially than the other. Nevertheless, these results confirm the formation of a di-octahedral smectite (montmorillonite) on the glass surface during vapor phase hydration in this study.

The composition of the phyllosilicates formed on AVM10-180 and AVM10-557 seem to differ, notably in Mg and O content. AVM10-180 sample has higher Mg and O contents. It is reasonable to suggest that the excess Mg and O in the AVM10-180 sample may be due to the presence of brucite (Mg(OH)₂), which is a well-known precursor of Mg-rich smectites [69-71]. No peaks were distinguishable in the XRD pattern, although the TEM images (figure 2(f) and supplementary data-figure S 3) clearly show the presence of a sheet-type mineral. The stoichiometric ratios suggest the possibility of either a di-octahedral smectite or a tri-octahedral smectite, depending on the incorporation of Al in tetrahedral sites or octahedral sites, respectively.

At this stage the exact composition of the smectite formed on AVM10 samples in this study cannot be affirmed with the available information. However, a possible smectite composition is proposed based on the EDX analyses of AVM10-557 (table 2) and the generic formula for tri-octahedral smectites proposed by Joly et al. [72]. This generic formula shown in equation 3.1.1.1 was earlier used by Arena et al. for identification of a phyllosilicate formed on nuclear waste glass simulant ISG in the presence of Fe and Mg (aqueous alteration, SA/V 20000 m⁻¹, 50°C, 511 days) [49]. "X" in equation 3.1.1.1 corresponds to cations other than Al that may occupy octahedral sites, such as Mg or Fe. The proposed composition is

$$[(\text{Si}_{3.85}\text{Al}_{0.15})((\text{Mg, Fe})_{2.13}\text{Al}_{0.87})\text{O}_{10}(\text{OH})_2]^{0.72+}[\text{Na}_{0.1}\text{Ca}_{0.1}]^{0.3+}.$$

$$[\text{Si}_{(4-a)}\text{Al}_a](\text{X}_{(3-b)}\text{Al}_b)\text{O}_{10}(\text{OH})_2]^{(a+b)-}[\text{X}_c\text{Na}_d\text{Ca}_e]^{(2c+d+2e)+} \quad (\text{Equation 3.1.1.1})$$

3.1.2 AVMV4 and QMg

The Si/Al ratio of the glass QMg is the same as the glass AVMV4. The SEM images of both the Mg-containing glasses showed some similarities (i) The altered surface showed the presence of thread-like carpet of precipitates along with μm sized cluster of fibrous precipitates in the SEM images of samples altered for 180 days (AVMV4-180 and QMg-180) (figure 3(c) and 3(a) respectively). The altered surface of the samples altered for 557 days (AVMV4-557 and QMg-557) showed the presence of holes of 400-500 nm in diameter and a gnawed appearance, with pit size of a few hundred nm, respectively (figure 3(d) and 3(b) respectively) (ii) The altered layers of all four samples were not visible in SEM, indicating that their thickness must be less than 100 nm. Irregularly altered zones were also not observed in the SEM images.

TEM images of cross-section of AVMV4-557 show the presence of a gel layer of approximately 80 nm thickness (figure 3(e) & (f) and Supplementary data, figure S11). Above this apparently homogeneous gel layer, a mixture of amorphous and crystalline phases is distributed across the 5 μm cross-section in varying thicknesses (200 nm to 20 nm). STEM image of QMg-180 showed an altered layer next to the pristine glass that appears homogeneous and is between 40-60 nm in thickness (figure 4(a)). On the surface of the altered layer, a layer of fibrous precipitates of 30-40 nm in thickness is present. The electron diffraction patterns obtained from TEM imaging did not show any fringes in the zone of precipitates, indicating that the precipitates are probably amorphous. The STEM-EDX analysis indicated that the amorphous precipitates and the gel layer in the surface are enriched in Mg and Na and depleted in Al, with respect to pristine glass (supplementary data-figure S 12).

3.1.3 Q

SEM images of Q altered for 180 days and 557 days (Q-180 & Q-557) do not show any recognizable secondary precipitates. TEM image of a micro-section of Q-180 shows the presence of a seemingly homogeneous altered layer of approx. 40 nm thickness (figure 4(b)). The pores that are visible on the altered layer-pristine glass interface were formed / enlarged during exposure of the sample to the electron beam.

3.1.4 QCa

SEM images of QCa altered for 180 days (QCa-180) show a few unidentified scattered precipitates on the surface. TEM image of QCa-180 shows the presence of an apparently homogeneous altered layer of approximately 80 nm (figure 5(a)). The difference in density between the pristine glass and gel layer seems to be higher than other glasses observed.

Figure 5(b) shows the SEM image of QCa altered for 557 days (QCa-557). The sample surface contained significantly more surface precipitates than QCa-180. There seems to be two types of secondary phases; clusters of pointed needle-like secondary phases and cuboid precipitates. Figure 5(c) shows the SEM image of sample cross-section. An altered layer of approx. 110-150 nm thickness is distinguishable due to the contrast difference between the layer and the pristine glass. Calcite was identified by XRD patterns on QCa-180 and QCa-557.

3.2 Behavior of elements in the altered layers (ToF-SIMS profiles)

Among all the characterization techniques presented in this study, ToF-SIMS and FTIR analyze the largest surface area of the sample in a uniform manner for all six samples. Therefore, it is considered to be the most suitable method for inter-comparison and the most representative in terms of element behavior in the altered layer and the average depth of altered zone. Table 3 summarizes and compares the thicknesses of the altered layers measured using ToF-SIMS and TEM images. The uncertainties of the given values could not be calculated. The percent error associated with ToF-SIMS measures is generally considered to be less than 3% [73]. Other factors contributing to the uncertainty are surface irregularity due to precipitates, constant speed of abrasion used for the entire zone of analysis and irregular/discontinuous altered zones. However, based on the coherence between the results of ToF-SIMS and other characterization techniques, it can be presumed that the uncertainty associated with the altered layer thicknesses can be overlooked.

Figure 6 presents the normalized ToF-SIMS profiles of the major elements present in the six glasses altered for 180 days. The normalized ToF-SIMS profiles of all the elements present in all six samples altered for 180 days and 557 days are presented in supplementary data (figures S 13 to S 19).

As observed in section 3.1, a similarity in the behavior of elements of the glasses AVM6 / AVM10 and AVMV4 / QMg is noticeable. The striking similarity in the behavior of H, B, Al, Na and Mg in the glasses AVMV4 and QMg are presented in supplementary data (figure S 20). Globally, for each glass, the behavior of elements in the altered layer is remarkably similar among the two different samples altered for two different durations. The four Mg-containing glasses show the presence of a layer of precipitates towards the surface of the altered layer. As in SEM images, the thickness of this precipitate layer is much higher in AVM6 (250-300 nm) and AVM10 (150-250 nm) than the AVMV4 and QMg glasses (<10 nm). This precipitate layer mainly contains Mg, Na, Li, Cs and Fe (in addition to Si).

The altered layer-pristine glass interface is rather sharp for the samples AVMV4, Q, QCa and QMg, unlike for the AVM6 and AVM10 samples. This apparently broad interface is due to the irregular and discontinuous altered zones observed in SEM images. Therefore the thickness estimated for these two glasses is considered as an average thickness of the analyzed zone. Based on the ToF-SIMS thickness (boron) from table 3, the glasses AVM6 and AVM10 alter 10-30 times faster than the other four glasses. Among the samples altered for 180 days, AVMV4, QCa and QMg alter 1.7 times faster than the glass Q. Among the samples altered for 557 days, QCa alters almost twice that of AVMV4, QMg and Q. In testing two samples of each glass for durations of 180 and 557 days, we considered that the rate of alteration would be similar. However, the increase in the thickness of altered layer from 180 days to 557 days suggests that the vapor hydration rate has decreased by a factor of 9.1 for AVMV4, 8.5 for QMg, 1.9 for Q and 1.6 for QCa after 180 days of alteration (considering that the vapor hydration rate is constant between 0-180 days and between 180-557 days).

In coherence with the STEM-EDX results, Al is depleted in the zone of surface precipitates of the Mg-containing glasses, indicating that the Si/Al ratio is higher in the phyllosilicate layer than the glass.

The ToF-SIMS profiles, which have been normalized to Si and to PG, might give an impression that many elements are depleted from the gel layer, even though not as extensively as boron. It seems likely that this depletion is due to a migration of the element towards the surface to form precipitates. In the zone of precipitates, the normalization with respect to Si creates an artificial depletion of elements such as Zr, rare-earths and Al, because they are almost absent in the precipitate layer, towards the surface. The elements which are really depleted (absent in gel layer and precipitate layer) are boron, Ca in QCa and Na from the surface of Q. The retention of Ca is < 3% in the gel layer of QCa (in both QCa-180 and QCa-557).

3.3 Porosity of the altered layer (SAXS)

The porosity, pore-size and specific surface area values reported in this paper were calculated by considering that the pores of the gel layer are filled with water. This assumption will be discussed later in section 4. The data treatment was based on previous works [62-64] and is explained in detail in the supplementary data (section1). q is the scattering vector in nm^{-1} and I_{corr} (cm^{-1}), calculated from equation S9 in supplementary data, separates the scattering intensity in the high q domain by the pores in the gel layer from the scattering in the low q domain by the grain envelopes.

AVM6 and AVM10: The plots of I_{corr} vs. q of these two glasses show a porod regime ($I_{corr} \propto q^{-4}$). The SAXS spectra of these glasses are provided in figure S 21 (supplementary data). In both glasses, the high q porod regime shifts to higher q values with time. However, porod's law cannot be used to calculate the porosity and specific surface area of pores for these two glasses, since the SEM images of the monolith samples indicate that these glass surfaces are covered with phyllosilicates. Therefore, the SAXS diagram contains information regarding both the porosity of the gel layer and the inter-layer spacing of the phyllosilicates and they cannot be deconvoluted.

AVM6 glass powders of particle size 2-5 μm that were prepared as described in section 2.1 were altered at 50°C and 95% RH for 11 days, 31 days and 90 days, for the purpose of characterization by SAXS and identification of possible trends in the evolution of the gel layer. These samples are referred to as AVM6-11, AVM6-31 and AVM6-90. The I_{corr} vs. q plots of these glasses are shown in figure S 22 (supplementary data). Porod's law is respected at higher q values for all three samples including the sample altered for only 11 days. The quantity of secondary phases on these samples altered for a short duration is negligible (TEM images (not shown here) of AVM6 samples altered for 90 days at 50°C and 95% RH show that the surface precipitates are visually much less denser than the AVM6-180 samples). Therefore, the porosity, pore-size and specific surface area of the gel layer can be calculated. The porosity, pore diameter and specific surface area of AVM6-11 are 66%, 4.4 nm and 328 m^2/g respectively; that of AVM6-31 are 47%, 4.5 nm and 235 m^2/g respectively; and that of AVM6-90 are 11%, 4.8 nm and 58.2 m^2/g . These values are recapitulated in table 4. It can be noticed that porosity decreases with time, while pore size increases. The I_{corr} vs. q plot of AVM6-11 is distinctly different than that of the other AVM6 samples. The shoulder corresponding to the highest intensity is at a higher q for the AVM6-11 sample. This translates to a smaller average pore size than the other glasses [74]. However, the porod regimes of the AVM6 samples altered for larger duration is shifted towards much higher q . This suggests the presence of smaller pores in the samples that were altered for a duration longer than 11 days, even though the average pore-size increases with increase in duration of alteration.

AVMV4 and QMg: I_{corr} vs. q plot of these two glasses are similar in the sense that, neither of them displays a porod's regime. The plots are shown in figure S 22 (supplementary data). The exponent D ($I(Corr) \propto q^{-D}$) decreases with increase in duration of alteration, suggesting an increase in the roughness of the pore-interface. It can be considered that the reason for the absence of a porod's regime in the SAXS diagram is the interference of poorly crystallized precipitates. This means that the D value, which varies between 3.4 to 2.6, is not representative of a rough pore-interface in the gel layer,

but rather a distortion of signal due to the presence of almost equal proportions of gel layer and poorly crystalline precipitates.

Q and QCa: The I_{corr} vs. q plot of these two glasses exhibit a porod's regime (figure 7). The absence of a substantial amount of secondary precipitates on the SEM and TEM images of the monolith samples validate the use of these measurements to calculate the porosity, pore size and specific surface area of pores. The porosity of Q-180 is 65% and decreases to 44% in the Q-557 sample. The pore diameter increases from 4.3 nm in the Q-180 sample to 5 nm in the Q-557 nm. The surface area of pores also decrease from 451 m²/g in the Q-180 sample to 264 m²/g in the Q-557 sample. The porosity of QCa-180 is 27%, which decreases to 9% in the QCa-557 sample. The pore diameter increases from 5.1 nm in QCa-180 to 7.5 nm in QCa-557. The surface area of pores decrease from 158 m²/g in QCa-180 to 37.6 m²/g in QCa-557. These calculated values are presented in table 4. Contrary to AVM6 and AVM10 samples altered for 180 days and 557 days each, the high q porod's regime shift towards lower q at longer duration of alteration. This indicates an increase in the average pore size with time. The higher pore sizes of the QCa sample than the Q sample and the factor of increase in pore-size with time correspond well with the magnitude of the shift in high- q porod's regime to lower q values for these samples as shown in figure 7.

3.4 Hydration kinetics

3.4.1 FTIR spectroscopy

The hydration kinetics is followed by studying the evolution of the increase in the absorbance of the band attributed to the OH stretching mode in SiOH molecules. For this, the absorbance around 3600 cm⁻¹ (OH stretching) measured at a given time of alteration (A) is reduced by the absorbance for the pristine glass (A_0). Figure 8 shows the increase of ($A-A_0$) over time for all the six glasses until 557 days of alteration. Figure 8(a) shows the difference in the increase of ($A-A_0$) versus time according to the glass stoichiometry. The increase in absorbance of AVM6 glass is approximately twice that of AVM10, 10 times that of QCa and 15 times that of AVMV4, Q and QMg. By correlating the increase in the absorbance of the SiOH band to the thickness of altered layer formed and the vapor hydration rate, it seems that there is an inflexion in the vapor hydration rate of all six glasses around approximately 6 months in the given conditions. For the AVM10 glass, it seems that this inflexion occurs at 4 months. In figure 8(d), it seems that there is acceleration in the vapor hydration rate between 60 and 120 days of alteration, followed by a strong slowdown of the vapor hydration rate. Figures 8(c) shows the strikingly similar behavior of the AVMV4 and QMg glasses. The inflexion seems to occur around 120 days of alteration. There also seems

to be a decrease in the absorbance after approximately 380 days of alteration. Figure 8(b) shows the evolution of $(A-A_0)$ vs. time of the glasses Q and QCa. The inflexion seems to occur approximately around 180 days for the samples Q, QCa and AVM6. The factor by which the rate of increase of $(A-A_0)$ drops after six months vary from 7.5 (AVM6) to 15 (AVM10).

3.4.2 Alteration kinetics based on the different measurements of thickness

The measurements of the thickness of the altered layers formed by ToF-SIMS and SEM/TEM images after 180 days and 557 days of vapor hydration of the six glasses are presented in table 3. It can be noticed that the thickness measured by ToF-SIMS is lower than the thickness measured by SEM/TEM images for four of the six glasses (AVMV4, Q, QCa and QMg). This is likely due to the fact that in ToF-SIMS, the layer of precipitates and the gel layer might get abraded faster than the pristine sample due to the difference in composition and their lower density. But the same speed of abrasion was used whatever the layer considered. As a result, the thicknesses of the altered layers, which are a combination of the gel layers and precipitate layers, are underestimated. Nevertheless, the thicknesses measured by ToF-SIMS and TEM images are in the same order of magnitude. A second similarity between the thicknesses measured by both techniques is that the sample Q has the smallest thickness among the four samples altered for 180 days and the thickness of the samples Q, QMg and AVMV4 are similar among the samples altered for 557 days. Therefore, it can be stated that the two techniques corroborate each other. In the case of the glasses AVM6 and AVM10, which have an irregular alteration, ToF-SIMS provides an average altered layer thickness in a relatively larger zone ($50 \times 50 \mu\text{m}^2$) and the SEM/TEM images have shown that the thickness could vary from a few tens of nm to a few μm . The average thickness provided by ToF-SIMS is useful to identify the relative durability of glasses. In addition, according to the FTIR results, the glasses AVM6 and AVM10 alter 10-20 times faster than the other four glasses. This result is very well corroborated by the ToF-SIMS results. While studying the alteration kinetics based on ToF-SIMS and SEM/TEM images, the rate of formation of altered layer (in nm/day) after 180 days and 557 days calculated by assuming linear alteration kinetics shows that the rate has decreased between 180 days and 557 days of vapor hydration. This result is also explained very well by the FTIR spectroscopy, which shows an inflexion in the rate of increase in $(A-A_0)$ with time after about 120-200 days of alteration. Thus the alteration kinetics measured by three different techniques are coherent.

4. Discussion

4.1 Morphology of the altered layer

Figure 9 shows a schematic description of the different morphologies of the altered layer for all six glasses altered under the same conditions. All six glasses present a homogeneous gel layer of tens of nm thickness adjacent to the pristine glass. AVM6 and AVM10 present irregularly shaped, discontinuous and more porous altered zones beneath the continuous gel layer. These two glasses contain significant amount of well-developed Mg-rich smectites and needle-shaped precipitates (AVM6 has more of it than AVM10). AVMV4 and QMg also present a layer of poorly-crystalline Mg-rich layer of precipitates on the surface above the gel layer. However, the SEM images have shown that they are present in a much lesser quantity than in AVM6 and AVM10. SEM images have not revealed any irregularly altered zones in these glasses. Q and QCa glasses also contain precipitates on the surface of the gel layer, but unlike in the Mg-containing glasses, they do not cover the glass surface. They are rather present in the form of crystals, which are either isolated or in clusters.

The morphology of AVM6 and AVM10 altered samples is rather surprising, particularly because of the presence of porous irregular altered zones beneath the homogeneous gel layer. Irregular alteration has been noticed in literature [75-78], especially in atmospheric alteration studies. The formation of a heterogeneous altered layer and craters are often attributed to a localized chemical attack due to surface defaults such as cracks/scratches/fissures or deposit of dust particles/matter from exposure to atmosphere or formation of hygroscopic salts locally on the surface or preferential/irregular water condensation [22, 79, 80]. The unexpected part was the presence of the uniform and continuous gel layer in-between phyllosilicates and irregular more porous discontinuous altered zones. A similar dense gel layer formed in-between phyllosilicates and irregular porous zones could not be found in literature. The closest analogy found was the gel layer formed during the aqueous alteration of a Si-B-Na-Ca-Zr glass. In the cited studies, a dense gel layer was present on the altered surface and above a porous gel layer. This denser gel layer was associated with pore-closure with time and passivating effect of the gel layer [81-83]. However, in literature, a denser gel layer close to the unaltered glass and a porous gel layer towards the glass surface and beneath secondary phases have been noticed [84]. Two possibilities can be imagined in our study: (i) The hydration front is irregular; the pore closure due to reorganization of the gel occurs at the surface in the region of the “oldest” gel, as suggested in the above mentioned example [83]. (ii) The denser gel layer and the irregular, more porous, discontinuous altered zones were

formed or driven by two different mechanisms. The second assumption seems more likely and is discussed further in section 4.5.

4.2 Behaviour of elements (alkalis, Ca and B) in the altered zone

Boron is depleted in the gel layer of all six glasses (less than 20% retention). Although it is useful to estimate the altered layer thicknesses from ToF-SIMS profiles, its depletion is puzzling. It would be logical to expect that elements are not lost from the altered layer during vapor phase hydration. The depletion could mean that there is water condensation on glass surface followed by run-off. If this is the case, the loss of other soluble elements such as Na and Li can be expected as well. However, Na is retained to a higher extent than boron as can be seen in figure 6. The profiles of B, Na and Li do not resemble each other. Therefore, the possibility of evaporation of boric acid species at 50°C and 95% RH should also be investigated [85, 86].

Hence, a vapor hydration experiment was conducted with 0.6 g of borosilicate glass (QMg) powder of particle size 20-40 μm (90°C, 98% RH, 153 days) using the protocol previously used on glass monoliths by Neeway et al. [28]. The glass powder was placed in a cup inside the reactor above NaCl solution that was used to impose relative humidity. The set-up was arranged in such a way that the water that condenses on glass powders in the cup cannot run-off. Despite the set-up, 0.7 ± 0.1 mg of boron was present in the NaCl solution at the end of the experiment. The vapor hydration rate of QMg at 90°C was estimated based on unpublished results and using this value, it was estimated that $27 \pm 6\%$ of boron from the altered layer was lost by evaporation. This experiment shows the possibility of evaporation of boron/boric acid species and indicates that at 50°C, probably only a small fraction of boron escapes due to volatility and a large fraction must be lost due to condensation and run-off.

Ca is depleted to a higher extent than boron in the QCa glass (<2% retention). It can be justified by the formation of calcite crystals on the surface of the glass, which may adhere poorly. For a glass that has only 52 nm thick altered layer, sufficient quantity of calcite had precipitated to be identified in XRD pattern. The depletion of Na towards the surface of the Q glass could probably be due to formation of carbonates (although undetected). In the other glasses, Na is well retained in the gel layer. In figure 6, a certain similarity can be observed in the profile of Na and H for all glasses. This suggests that Na is reactive and might be linked to inter-diffusion reaction. Despite being probably released from the glass network, Na is still well retained in the gel layer (except in Q). It may be present in porewater, form

precipitates or may participate in the hydrolysis of $\equiv\text{Si-O-Si}\equiv$ bonds to form $\equiv\text{Si-O}^-\dots\text{Na}^+$ bonds, as suggested in literature [39].

4.3 Porosity of the altered layer

During the SAXS data treatment, it was assumed that the pores in the gel layer are filled with water. This assumption is supported by the calculation of the threshold pore-size by Kelvin's equation (equation 4.3.1) [87], below which, water is expected to condense in pores due to capillary effect. This threshold pore-radius was calculated to be 9.2 nm at 50°C and 95% RH from equation 4.3.1. The maximum value of the pore-radius measured through SAXS is <4 nm. Therefore, it seems highly probable that the pores are filled with water. The porosity of the gels was also calculated by considering that the pores are filled with air, but in this case, the calculated porosity values were unrealistic. This further reinforces our assumption that the pores are filled with water. However, a certain uncertainty is associated with this assumption. Even if it is considered that the pores are indeed filled with water during the experiment, it is unclear if the water stays in the pores during characterization or it evaporates/escapes into the atmosphere once the sample is removed from the humid and hot atmosphere (95% RH & 50°C). Data analysis has been carried out despite this uncertainty by considering that water remains inside the pores, since the samples were not exposed to high temperatures or desiccators during storage until characterization. Specific studies to carefully assess the impact of this uncertainty on data treatment are a necessary perspective.

$$\ln \frac{P}{P_0} = -\frac{2\gamma V_l}{RT} \quad (\text{Equation 4.3.1})$$

The values of the porosity, specific surface area of the pores and the pore-radiuses are in the same order of magnitude as those observed in published aqueous alteration experiments of borosilicate glasses [63, 88, 89]. 66% porosity of the gel layer of Q-180 and AVM6-11 (table 4) seem relatively high, especially while comparing with TEM images of Q-180, which do not show a very porous altered layer. This means that either the porosity measured by SAXS is overestimated or there is some other unknown mechanism that could explain such high porosity values, which needs further investigation of the gel layer formed on these glasses. This porosity value may be overestimated due to the volume fraction of gel used in data treatment, which is reasonably assumed based on altered layer thicknesses of the gel layer formed on monoliths. This being said, such high porosity values have also been reported during aqueous alteration of glasses [63, 89].

From table 4, all three glasses show a decrease in porosity and surface area of pores with time and an increase in the average pore size with time. This evolution in our vapor hydration study is similar to the results of an aqueous alteration study conducted by Girard et al., who altered glasses containing Si, B, Na, Ca and Zr in aqueous medium at an SA/V (surface area of glass/solution volume) ratio of 3000 m⁻¹ at 90°C for time periods up to 96 h [89]. According to their results, the porosity, depending on composition, increased rapidly to a maximum value within a few hours of glass alteration. After reaching maxima, the porosity and specific surface area of pores decreased with increasing time of alteration, probably due to a shrinking gel and the pore-size increased due to either coalescence of pores or further dissolution at the pore walls. The initially high porosity after a few hours of glass leaching was attributed to leaching of Si from the solution without re-condensation until the solution becomes saturated with respect to Si. This theory was based on the calculation of an estimated porosity from leachate composition. In this study, the leachate cannot be sampled since it is a vapor phase alteration. Therefore, an acceptable estimated porosity cannot be calculated using the leached fraction of soluble elements such as B and Na, as was done in literature [89]. However, an estimated porosity was calculated based on the retention factor R of elements in the gel layer calculated from ToF-SIMS profiles of monoliths and the volume fraction occupied by oxides ϕ_i as shown in section 8 of the supplementary data.

The estimated porosity values thus calculated vary between 14% and 25% (table S 1-supplementary data). For all six glasses, the estimated porosity value at 557 days is less than the estimated porosity value at 180 days. This decrease in this estimated porosity is coherent with the SAXS results. Nevertheless, the values of porosity calculated by SAXS for the glass Q is 3.2 to 3.9 times higher than the hypothetical values estimated by depleted elements (based on ToF-SIMS results). It can be supposed that the porosity estimated by retention of elements in the gel layer calculated based on ToF-SIMS analysis is probably underestimated, because it considers that the elements present in the porewater of the gel layer are a part of the gel layer network. There is the possibility of overestimation of porosity values by SAXS as well. In the cases in which the SAXS porosity is lower than the porosity estimated from SIMS data, different hypotheses such as a shrinking gel or precipitation of colloids or secondary phases (calcite) in the pores could be proposed based on literature [89, 90].

4.4 Hydration Kinetics

Overall, the relative durability of the glasses identified by the increase in absorbance of the SiOH molecules in FTIR spectra are coherent with that measured by other characterization techniques. These results reinforce the argument that FTIR spectroscopy is a good method to follow vapor hydration

kinetics, in the absence of sampling techniques to determine soluble element concentrations in the leachate. All glasses showed an inflexion in the vapor hydration kinetics after 120 or 180 days of alteration. The cause for this inflexion has not yet been investigated. But such inflexion has been observed earlier in literature, notably in the experiments conducted on CSD-B (inactive simulant of intermediate-level long lived waste glass) and SON68 glasses after about 100-200 days of alteration (at 35-90°C) [29, 58].

4.5 Influence of glass composition and insights into vapor hydration mechanisms

The difference in the vapor hydration kinetics of AVM6, AVM10 and AVMV4 is an indication of the significant effect of glass composition on glass hydration. The effect of stoichiometry on the relative durability of AVM glasses in aqueous medium was already investigated [46, 47]. According to these studies, the three major parameters affecting glass durability in water under a given condition were pH, Mg and Al concentration. When $\text{pH}_{50^\circ\text{C}} > 9$, alteration rates increase due to precipitation of Mg-aluminosilicates. Moreover, AVM glasses contain very little Ca. Therefore, it is considered that the role of charge compensating atoms of $[\text{AlO}_4]^-$ units is preferentially occupied by Mg (the preference in gels decreases in the order $\text{Ca}^{2+} > \text{Mg}^{2+} > \text{Na}^+$). Thus, a higher quantity of Al in the gel layer probably retains higher quantity of Mg in the gel, thereby, increasing the passivation properties of the gel layer [46, 47]. This interpretation was used to explain the highest relative durability of AVM10 glass in aqueous medium, since it contains the highest Al concentration among the three glasses.

In our vapor hydration study, AVM10 glass is one of the two least durable glasses. Therefore, the glass durability is not simply linearly dependent on Al concentration. The reason for this could be that the AVM10 glass contains higher MgO molar concentration than Al_2O_3 (i.e. molar ratio of $\text{Al}_2\text{O}_3/\text{MgO} < 1$). Therefore, as an extreme case, if it is considered that all the $[\text{AlO}_4]^-$ units in the gel layer are charge compensated by Mg^{2+} ions, there is still an excess of Mg that can saturate the molecular water layers/porewater to form Mg-silicates, thus driving the glass alteration. The difference in the relative durability of AVM10 between aqueous medium and vapor phase could be due to the possibly higher pH of the very small volume of water in vapor phase, thereby promoting the precipitation of Mg-silicates during vapor hydration and not as much during aqueous alteration.

The lower durability of AVM6 glass in this vapor hydration study can also be explained using the same interpretation (i.e. molar ratio of $\text{Al}_2\text{O}_3/\text{MgO} < 1$). The extensive alteration of AVM6 and AVM10, which is manifested as irregularly altered zones, could be driven by the precipitation of a significant amount of Mg-silicates. On the other hand, this ratio is equal to 1 for AVMV4 and is greater than 1 for QMg,

suggesting that, Mg could be principally occupying the role of charge compensating atom and therefore be less available for participation in the formation of secondary phases. As a result, the vapor hydration of these two glasses may not be accelerated due to the precipitation of Mg-silicates.

The lack of structural study to support this assumption definitely needs to be acknowledged. The distribution of coordination number of Al in the gel layer was not studied. Incidentally, recent publications have shown that due to the high cation field strength of Mg, the presence of this element in the glass network increases the fraction of $^{(v)}\text{Al}$ and $^{(vi)}\text{Al}$ and $^{(iii)}\text{B}$, and thus contributes to glass depolymerisation [91, 92]. As a matter of fact, the fraction of $^{(iv)}\text{B}$ in the Mg containing glasses in our study were lower than that in the glasses Q and QCa (section 2.1). It is also suggested that some of the Mg could be acting as a network former [92]. Therefore, there is a need to better understand the role of Mg in the glass as well as in the gel, its impact on the gel structure and especially the competition between ions to compensate the charge of $[\text{AlO}_4]^-$ units.

In order to understand the specific effect of Ca and Mg on vapor hydration of glasses, the results of the simplified glasses Q, QCa and QMg need to be focused upon. Table 3 shows that QCa and QMg alter 1.6 to 1.7 times faster than Q, among the samples altered for 180 days. This can be construed to be a negative effect of Ca and Mg, due to the precipitation of calcite and Mg-rich precipitates. However, the NBO fraction (table 1) indicates that these two glasses have higher fraction of NBOs than the glass Q. From figure S 23 in supplementary data, it can be seen that, among the glasses altered for 180 days, the higher the NBO fraction, the higher the thickness of the altered layer formed. This relation seems to be linear for the glasses AVMV4, Q, QCa and QMg and a sharp rise is noted for the glasses AVM6 and AVM10, which have undergone extensive alteration due to secondary phases precipitation. Therefore, the slightly higher altered layer thicknesses of the glasses QCa and QMg in comparison to Q could be due to the lower resistance to network hydrolysis and not a negative effect of Ca or Mg. This suggests that network-hydrolysis could be the rate limiting mechanism of formation of the uniform gel layer.

Among the samples altered for 557 days, the altered layer thickness of QCa is twice that of Q and QMg. This change in the relative durability of glasses with a longer duration can be explained by considering the presence of a passivating altered layer. The SAXS results also hint at a reorganization of the homogeneous gel layer, at least in the case of Q, QCa and AVM6. The inflexion in the vapor hydration kinetics (FTIR spectroscopy) after 180 days approximately strongly suggests the presence of a passivation

mechanism of the gel layer in all six glasses. After six months, the altered layer of QMg (and AVMV4) could have become more passivating than that of Q and QCa. This presumption is based on ToF-SIMS profiles, which show that the retention of Ca in the gel layer is less than 1% and Na is less retained in the gel layer of Q. The gel layer of QMg (and AVMV4) retains a higher quantity of Mg. It has already been shown that the retention of Mg increases the passivation properties of the gel layer [46]. This implies that the rate-limiting vapor hydration mechanism changes, probably to diffusion of species through the gel layer, after the inflexion of vapor hydration rate due to the formation of a passivating altered layer. This is in agreement with the structure discussion above for AVMV4 and QMg.

In brief, the specific effect of Ca or Mg could not be seen in this vapor hydration study because the excessive concentration of Al (molar ratio of $\text{Al}_2\text{O}_3/(\text{MgO or CaO}) \geq 1$) has masked the possible negative effect that Ca or Mg could have due to secondary phase precipitation. The presence of Al in the glass increases its resistance to network hydrolysis since $\equiv\text{Si-O-Al}\equiv$ bonds require more energy to be broken than $\equiv\text{Si-O-B-}$ or $\equiv\text{Si-O-Si}\equiv$ bonds [54, 93].

The interpretation of the results suggests that the rate-limiting mechanism of formation of the gel layer in vapor hydration is network hydrolysis in this study. This conclusion is reinforced by the fact that AVM10, which has the highest Al content in the pristine glass, has the lowest thickness of the homogeneous gel layer (15-30 nm in TEM), even if the overall alteration layers cumulate to larger thickness after secondary phases form.

The formation of irregularly shaped (few tens of nm to few μm thick), discontinuous, more porous altered zones behind the homogeneous gel layer in AVM6 and AVM10 glasses seem to be driven by precipitation of significant quantities of Mg-silicates. During vapor hydration, extensive alteration due to secondary phase precipitation is naturally local (and hence irregular). Thus, it is possible that in AVM6 and AVM10, the two types of altered zones were formed by two parallel mechanisms.

The precipitated secondary phases found at the surface in the other four glasses (AVMV4, Q, QCa and QMg) are probably a consequence of the release of alkaline-earth elements from glass network and do not drive the formation of their homogeneous gel layer.

4.6 Vapor hydration vs. aqueous alteration

Glass AVM6 was found to be the glass of lowest durability of the series in aqueous leaching and in the present vapor phase alterations. However, a reversal of glass durability in vapor phase and aqueous medium has been observed between the glasses AVM10 and AVMV4. The residual alteration rates of the three complex glasses in aqueous medium (initially pure water, 50°C, $\text{SA/V}=5500 \text{ m}^{-1}$, values measured between 5-10 years of alteration) are: AVM6- $5.1 \times 10^{-4} \text{ g/m}^2/\text{day}$; AVM10- $9 \times 10^{-5} \text{ g/m}^2/\text{day}$; [46]; AVMV4-

5.6x10⁻⁴ g/m²/day (personal communication-value estimated based on a statistic interpolation model). The difference may be due to changes in the solution chemistry of the very low volume of water available for glass dissolution in vapor phase. This small volume of water may get rapidly saturated with respect to secondary phases that are clearly different than those that precipitate during aqueous alteration.

The smectites formed during vapor hydration, as identified through STEM-EDX analyses (see sub-section of 3.1.1), seem to be different than those that form during aqueous alteration of the same glasses. A tri-octahedral smectite was identified on AVM6 altered in aqueous medium [46], while a di-octahedral smectite (type montmorillonite) was identified during this vapor hydration study of AVM6. The phyllosilicate formed in vapor phase contained 75% lower Al, 40% lower Mg and 10 times higher Fe content.

The phyllosilicate composition obtained on AVM10 in this study was compared with the phyllosilicate composition obtained during the aqueous alteration of AVM10 in the study conducted by Thien et al. (SA/V 5500 m⁻¹, 50°C, 2500 days, initially pure water and 400 mg/L of MgCl₂·6H₂O added after 114 days) [94]. The concentration of Al in the phyllosilicate of our study was 25% lower than the Al concentration in the smectite identified by Thien et al [94]. Similarly, the concentration of Mg was 30% lower and the concentration of Fe was three times higher.

This shows that caution needs to be taken while extrapolating aqueous alteration results to vapor hydration by considering that vapor hydration is equivalent to aqueous alteration at a very high SA/V ratio. Certain studies conducted vapor hydration tests in extreme conditions (150-200°C, 100% RH) to predict the secondary phases that would form during long-term aqueous alteration of glasses [36]. Here, it is clearly shown that the same phases do not precipitate in both media.

One similarity between aqueous alteration and vapor hydration studies of glasses is the texture of the gel layer. SAXS data indicated that the porosity, pore-size and specific surface area values are in the same order of magnitude and evolve similarly with time in the two glasses of different compositions and in different alteration conditions [88, 95]. This could imply a similar mechanism of formation of the gel layer.

5. Conclusion

In order to study the influence of glass composition on vapor hydration kinetics, three complex glasses (>20 oxides) and three simplified glasses (4 or 5 oxides) were altered in vapor phase (at 50°C and 95%

RH) for a period of 180 days and 557 days. Based on the analysis of the characterization results of the altered samples, it seems that network hydrolysis is the rate limiting mechanism of formation of the gel layer during vapor hydration of these glasses. Under conditions that are favorable for the precipitation of secondary phases, it seems that the vapor hydration kinetics is accelerated in a localized manner, leading to the formation of irregularly shaped, discontinuous altered zones that could be up to a few μm thick. The presence of alkaline-earth elements (such as Mg or Ca) seems to make the glass more reactive, since they actively participate in the formation of secondary phases. However, the negative effect of these elements is attenuated by the presence of Al, since Al increases the resistance to hydrolysis of glass network and its presence in the gel layer retains alkaline-earth elements to compensate $[\text{AlO}_4]^-$ entities. Therefore, when the molar ratio of $\text{Al}_2\text{O}_3/(\text{MgO or CaO}) \geq 1$, the positive effect of Al prevails over the expected negative effect of Ca or Mg and therefore the glass is relatively more durable. When the ratio is < 1 , the negative effect of Ca or Mg prevails. For this reason no specific effect of Ca or Mg on vapor hydration of the three simplified glasses could be seen (molar ratio of $\text{Al}_2\text{O}_3/(\text{MgO or CaO}) \geq 1$).

Apart from this principal result, two types of altered layer morphologies have been identified. The porous texture of the gel layer of a vapor hydrated glass has been investigated using SAXS. The measured pore-diameters vary between 4.3-7.5 nm, similar to the pore-sizes found in the gel layer formed on various similar glasses during aqueous alteration.

It has been shown that the vapor hydration mechanism changes with glass composition and time. The rate of vapor hydration evaluated in FTIR showed a decrease between 180 days and 300 days, which validate the formation of a passivating layer.

Based on this study, a few perspectives have been identified. The structural role of Mg in the glass and gel and its capability to compensate negative charge of $[\text{AlO}_4]^-$ units needs to be investigated to understand the positive effect of Al that prevails over the negative effect of Mg on glass durability. Aqueous alteration of the same glasses at very basic pH ($\text{pH}_{50^\circ\text{C}} > 11$) may provoke the precipitation of similar secondary phases in order to observe the relative durability of these glasses. This might help to affirm or refute the hypothesis of importance of molar ratio of $\text{Al}_2\text{O}_3/\text{MgO}$ on glass durability.

It would also be interesting to conduct vapor hydration experiments of the same glasses at a higher temperature ($> 90^\circ\text{C}$) to study if possibly favorable conditions for secondary phase precipitation drives vapor hydration or if the rate-controlling mechanism is network-hydrolysis as in low temperatures (50°C). It is also necessary to investigate if the gel layers formed during vapor hydration have any

protective effect against aqueous alteration, since it is expected that a vapor hydrated nuclear waste glass would eventually be altered in groundwater of the repository site.

Acknowledgements

We would like to thank Laurent Duffours (PrimeVerre) for preparation of the polished glass monoliths, Géraldine Parisot (CEA) for ICP-OES analysis of glass powders, Jean-Pierre Mestre (CEA) and Marie Fenart (CEA) for the SEM images, Myriam Chartier (CEA) for XRD patterns, Laurent Dupuy and Elodie Chauvet (TESCAN Analytics) for the ToF-SIMS profiles and Jeremy Causse (ICSM) for SAXS data acquisition. This study was supported by CEA and EDF (Electricité de France). We would like to particularly thank Florent Tocino and Hélène Schneider (EDF) for their support. We also thank the two anonymous reviewers for their helpful comments and constructive feedback.

Data Availability

The SEM and TEM data supporting the findings are available within the article and the supplementary information. The processed data of SAXS, ToF-SIMS, NMR spectroscopy and XRD apparatuses are also available within the article and supplementary information. The raw data of SAXS, ToF-SIMS, NMR spectroscopy and XRD apparatuses required to reproduce these findings cannot be shared at this time due to technical and time limitations. However, they can be shared by the corresponding author upon reasonable request.

References

1. Friedman, I. and W.D. Long, *Volcanic glasses, their origins and alteration processes*. Journal of Non-Crystalline Solids, 1984. **67**: p. 127-133.
2. Verney-Carron, A., S. Gin, and G. Libourel, *A fractured roman glass block altered for 1800 years in seawater: Analogy with nuclear waste glass in a deep geological repository*. Geochimica et Cosmochimica Acta, 2008. **72**(22): p. 5372-5385.
3. ANDRA-Collectif, *Dossier d'options de sûreté - Partie après fermeture (DOS-AF)*. 2016, ANDRA. p. 1-467.
4. Poinssot, C. and S. Gin, *Long-term Behavior Science: The cornerstone approach for reliably assessing the long-term performance of nuclear waste*. Journal of Nuclear Materials, 2012. **420**(1-3): p. 182-192.
5. De Echave, T., et al., *Influence of iron on the alteration of the SON68 nuclear glass in the Callovo-Oxfordian groundwater*. Applied Geochemistry, 2019. **100**: p. 268-278.
6. De Echave, T., et al., *Effect of clayey groundwater on the dissolution rate of SON68 simulated nuclear waste glass at 70 °C*. Journal of Nuclear Materials, 2018. **503**: p. 279-289.
7. Suzuki-Muresan, T., et al., *Alteration of vitrified intermediate level nuclear waste in alkaline media: effects of cementitious materials, pH and temperature*. RSC Advances, 2018. **8**(66): p. 37665-37680.

8. Rieke, P.C., et al., *Adaptation of the GRAAL model of Glass Reactivity to accommodate non-linear diffusivity*. Journal of Nuclear Materials, 2018. **512**: p. 79-93.
9. Frugier, P., et al., *Modeling glass corrosion with GRAAL*. npj Materials Degradation, 2018. **2**(1): p. 35.
10. Ducasse, T., et al., *Alteration of synthetic basaltic glass in silica saturated conditions: Analogy with nuclear glass*. Applied Geochemistry, 2018. **97**: p. 19-31.
11. Gin, S., et al., *Atom-Probe Tomography, TEM and ToF-SIMS study of borosilicate glass alteration rim: A multiscale approach to investigating rate-limiting mechanisms*. Geochimica et Cosmochimica Acta, 2017. **202**: p. 57-76.
12. Collin, M., et al., *Structure of International Simple Glass and properties of passivating layer formed in circumneutral pH conditions*. npj Materials Degradation, 2018. **2**(1): p. 4.
13. Grambow, B. and R. Muller, *First-order dissolution rate law and the role of surface layers in glass performance assessment*. Journal of Nuclear Materials, 2001. **298**(1,2): p. 112-124.
14. Hellmann, R., et al., *Nanometre-scale evidence for interfacial dissolution-precipitation control of silicate glass corrosion*. Nature Materials, 2015. **14**(3): p. 307-311.
15. Geisler, T., et al., *Aqueous corrosion of borosilicate glass under acidic conditions: A new corrosion mechanism*. Journal of Non-Crystalline Solids, 2010. **356**(28-30): p. 1458-1465.
16. Ebert, W.L., R.F. Hoburg, and J.K. Bates, *The sorption of water on obsidian and nuclear waste glass*. Phys. Chem. Glasses, 1991. **32**(4): p. 133-137.
17. Gong, W.L., et al., *Secondary phase formation and the microstructural evolution of surface layers during vapor phase alteration of the French SON68 nuclear waste glass at 200°C*, in *Scientific Basis for Nuclear Waste Management XIX*, W.M. Murphy and D.A. Knecht, Editors. 1996, Mater. Res. Soc: Philadelphia, PA, USA. p. 197-204.
18. Bates, J.K., M.G. Seitz, and M.J. Steindler, *The relevance of vapor phase hydration aging to nuclear waste isolation*. Nuclear and Chemical Waste Management, 1984. **5**: p. 63-73.
19. Bates, J.K., et al., *Issues affecting the prediction of glass reactivity in an unsaturated environment*. Journal of Nuclear Materials, 1992. **190**: p. 198-227.
20. Bates, J.K., et al., *The hydration alteration of a commercial nuclear waste glass*. Chemical Geology, 1985. **51**(1): p. 79-87.
21. Abrajano, T., J.K. Bates, and C.D. Byers, *Aqueous corrosion of natural and nuclear waste glasses I. Comparative rates of hydration in liquid and vapor environments at elevated temperatures*. Journal of Non Crystalline Solids, 1986. **84**: p. 251-257.
22. Abrajano, T.A., Jr., J.K. Bates, and J.J. Mazer, *Aqueous corrosion of natural and nuclear waste glasses. II. Mechanisms of vapor hydration of nuclear waste glasses*. Journal of Non-Crystalline Solids, 1989. **108**: p. 269-288.
23. Gong, W.L., et al., *Analytical electron microscopy study of surface layers formed on the French SON68 nuclear waste glass during vapor hydration at 200°C*. Journal of Nuclear Materials, 1998. **254**(2): p. 249-265.
24. Pierce, E.M., et al., *The Accelerated Weathering of a Radioactive Low-Activity Waste Glass Under Hydraulically Unsaturated Conditions: Experimental Results from a Pressurized Unsaturated Flow Test*. Nuclear Technology, 2006. **155**(2): p. 149-165.
25. McKeown, D.A., et al., *Tc and Re Behavior in Borosilicate Waste Glass Vapor Hydration Tests*. Environmental Science & Technology, 2007. **41**(2): p. 431-436.
26. Buechele, A.C., et al., *Tc and Re behavior in borosilicate waste glass vapor hydration tests II*. Journal of nuclear materials, 2012. **429**(1-3): p. 159-165.
27. Cassingham, N.J., et al., *Alteration layer formation of Ca- and Zn-oxide bearing alkali borosilicate glasses for immobilisation of UK high level waste: A vapour hydration study*. Journal of Nuclear Materials, 2016. **479**: p. 639-646.

28. Neeway, J., et al., *Vapor hydration of SON68 glass from 90 °C to 200 °C: A kinetic study and corrosion products investigation*. Journal of Non Crystalline Solids, 2012. **358**(21): p. 2894-2905.
29. Chaou, A., et al., *Vapor hydration of a simulated borosilicate nuclear waste glass in unsaturated conditions at 50 °C and 90 °C*. RSCC Advances, 2015. **5**(64538).
30. Chaou, A., et al., *The role of pH in the vapor hydration at 175 °C of the French SON68 glass*. Applied Geochemistry, 2017. **76**: p. 22-35.
31. Bouakkaz, R., A. Abdelouas, and B. Grambow, *Kinetic study and structural evolution of SON68 nuclear waste glass altered from 35 to 125 °C under unsaturated H₂O and D₂O¹⁸ vapour conditions*. Corrosion Science, 2018. **134**: p. 1-16.
32. Abdelouas, A., et al., *A Preliminary Investigation of the ISG Glass Vapor Hydration*. INTERNATIONAL JOURNAL OF APPLIED GLASS SCIENCE, 2013. **4**(4): p. 307-316.
33. Chaou, A.A., et al., *The French SON68 glass vapor hydration under different atmospheres*. Procedia Materials Science, 2014. **7** p. 179 – 185.
34. Collectif, *Référentiel du comportement des colis de déchets HA-MAVL - Tome 2 - Déchets vitrifiés*, ANDRA and CEA, Editors. 2012. p. 1-548.
35. Ebert, W.L. and J.K. Bates, *The reaction of synthetic nuclear waste glass in steam and hydrothermal solution*. 1990, United States: Materials Research Society.
36. Ebert, W.L., J.K. Bates, and W.L. Bourcier, *The hydration of borosilicate waste glass in liquid water and steam at 200° C*. Waste Management, 1991. **11**: p. 205-221.
37. Moriya, Y. and M. Nogami, *Hydration of silicate glass in steam atmosphere*. Journal of Non-Crystalline Solids, 1980. **38**: p. 667-672.
38. Wronkiewicz, D.J., J.E. Young, and J.K. Bates, *Effects of alpha and gamma radiation on glass reaction in an unsaturated environment*, in *Scientific Basis for Nuclear Waste Management*. 1991, Mater. Res. Soc. p. 99-106.
39. Alloteau, F., et al., *New insight into atmospheric alteration of alkali-lime silicate glasses*. Corrosion Science, 2017. **122**: p. 12-25.
40. Sessegolo, L., et al., *Long-term weathering rate of stained-glass windows using H and O isotopes*. npj Materials Degradation, 2018. **2**(1): p. 17.
41. Gentaz, L., et al., *Role of secondary phases in the scaling of stained glass windows exposed to rain*. Corrosion Science, 2016. **109**: p. 206-216.
42. Kudriavtsev, Y., et al., *Water vapor interaction with borosilicate glass*. Solid State Ionics, 2018. **321**: p. 122-125.
43. Bunker, B.C., *Molecular mechanisms for corrosion of silica and silicate glasses*. Journal of Non-Crystalline Solids, 1994. **179**: p. 300-308.
44. Kudriavtsev, Y., R. Asomoza-Palacio, and L. Manzanilla-Naim, *Interaction of water vapor with silicate glass surfaces: Mass-spectrometric investigations*. Technical Physics Letters, 2017. **43**(5): p. 447-449.
45. Cunnane, J.C., et al., *High-level nuclear-waste borosilicate glass : a compendium of characteristics.*, in *Scientific Basis for Nuclear Waste Management XVI*, C.G. Interrante and R.T. Pabalan, Editors. 1993, Mater. Res. Soc.: Pittsburgh, PA. p. 225-232.
46. Thien, B., et al., *The dual effect of Mg on the long-term alteration rate of AVM nuclear waste glasses*. Journal of Nuclear Materials, 2012. **427**: p. 297-310.
47. Thien, B., *Développement des bases théoriques nécessaires à la modélisation de la vitesse résiduelle d'altération en milieu aqueux des verres nucléaires AVM*. 2010, Université Montpellier II. p. 244.
48. Arena, H., et al., *Impact of Zn, Mg, Ni and Co elements on glass alteration: Additive effects*. Journal of Nuclear Materials, 2016. **470**: p. 55-67.

49. Aréna, H., et al., *Impact of iron and magnesium on glass alteration: Characterization of the secondary phases and determination of their solubility constants*. Applied Geochemistry, 2017. **82**: p. 119-133.
50. Aréna, H., et al., *Impact of Fe, Mg and Ca elements on glass alteration: Interconnected processes*. Geochimica et Cosmochimica Acta, 2018. **239**: p. 420-445.
51. Mercado-Depierre, S., et al., *Antagonist effects of calcium on borosilicate glass alteration*. Journal of Nuclear Materials, 2013. **441**(1-3): p. 402-410.
52. Jollivet, P., et al., *Effect of clayey groundwater on the dissolution rate of the simulated nuclear waste glass SON68*. Journal of Nuclear Materials, 2012. **420**: p. 508-518.
53. Jegou, C., S. Gin, and F. Larche, *Alteration kinetics of a simplified nuclear glass in an aqueous medium: effects of solution chemistry and of protective gel properties on diminishing the alteration rate*. Journal of Nuclear Materials, 2000. **280**(2): p. 216-229.
54. Gin, S., et al., *Effect of composition on the short-term and long-term dissolution rates of ten glasses of increasing complexity from 3 to 30 oxides*. Journal of Non-Crystalline Solids, 2012. **358**(18-19): p. 2559-2570.
55. Gin, S., Abdelouas, A., Criscenti, L.J., Ebert, W.L., Ferrand, K., Geisler, T., Harrison, M.T., Inagaki, Y., Mitsui, S., Mueller, K.T., Marra, J.C., Pantano, C.G., Pierce, E.M., Ryan, J.V., Schofield, J.M., Steefel, C.I., Vienna, J.D., *An international initiative on long-term behavior of high-level nuclear waste glass*. Materials Today, 2013. **16**(6): p. 243-248.
56. Trotignon, L., et al., *The compared aqueous corrosion of four simple borosilicate glasses: Influence of Al, Ca, and Fe on the formation and nature of secondary phases*. Journal of Nuclear Materials, 1992. **190**: p. 228-246.
57. Neeway, J., *The alteration of the SON68 reference waste glass in silica saturated conditions and in the presence of water vapor*. 2010, Université de Nantes. p. 205.
58. Bouakkaz, R., *Altération aqueuse et hydratation en phase vapeur du verre SON68 à basse température (35-90°C)*. 2014, L'Université Nantes Angers Le Mans.
59. Peña, F.d.l., et al., *hyperspy/hyperspy v1.4.1*. 2018.
60. Collin, M., et al., *Impact of alkali on the passivation of silicate glass*. npj Materials Degradation, 2018. **2**(1): p. 16.
61. Angeli, F., et al., *Structure and Chemical Durability of Lead Crystal Glass*. Environmental Science & Technology, 2016. **50**(21): p. 11549-11558.
62. Spalla, O., S. Lyonard, and F. Testard, *Analysis of the small-angle intensity scattered by a porous and granular medium*. Journal of Applied Crystallography, 2003. **36 part 32**: p. 338-347.
63. Spalla, O., et al., *Influence of insoluble elements on the nanostructure of water altered glasses*. Journal of Non-Crystalline Solids, 2004. **347**(1-3): p. 56-68.
64. Cailleteau, C., *Influence de la morphologie du gel sur la cinétique d'altération des verres nucléaires: rôle du calcium et du zirconium*. 2008, Thèse de l'école polytechnique de Paris.
65. Thien, B.M.J., *A simple way to constrain the stoichiometry of secondary smectites upon aqueous glass alteration*. Applied Geochemistry, 2014. **42**: p. 45-46.
66. Jolyon, R. and I. Chau, *Mindat : base de données minéralogiques*, in <http://www.mindat.org/>. 2013.
67. Bailey, S.W., *Crystal Structures of Clay Minerals and Their X-ray Identification*. Mineralogical Society, London, 1980. **Monograph 5**: p. 1-123.
68. Brindley, G.W. and G. Brown, *Crystal Structures of Clay Minerals and their X-ray identification*. Mineralogical Society, London, 1980. **Monograph 5**: p. 169-180.
69. Klopogge, J.T., S. Komarneni, and J.E. Amonette, *Synthesis of smectite clay minerals a critical review*. Clays and Clay Minerals, 1999. **47**(5): p. 529-554.

70. Harder, H., *The role of magnesium in the formation of smectite minerals*. Chemical Geology, 1972. **10**(1): p. 31-39.
71. Pascua, C.S. and H. Yamada, *LOW-TEMPERATURE FORMATION OF CLAY MINERALS : CORRELATING LABORATORY EXPERIMENTS WITH NATURAL FIELD-SCALE PROCESSES*. Clay Science, 2012. **16**(2): p. 25-32.
72. Joly, J.-F., et al., *Phyllosilicates 2:1 trioctaédriques et leur procédé de préparation*, E.P. Office, Editor. 1991, IFP Energies Nouvelles France.
73. Py, M., *Study of interfaces and nanometric structures by ToF-SIMS : upon a spatially resolved quantitative analysis*, in *Micro and nanotechnologies/Microelectronics*. 2011, Université de Grenoble.
74. Romanos, G.E., et al., *Methods of evaluating pore morphology in hybrid organic-inorganic porous materials*. Microporous and Mesoporous Materials, 2009. **120**(1): p. 53-61.
75. Alloteau, F., *Contribution à la compréhension des mécanismes de l'altération atmosphérique des verres et étude d'un traitement de protection à base de sels de zinc. Application à la conservation des objets en verre du patrimoine culturel*. 2017, l'Université de recherche Paris Sciences et Lettres PSL Research University.
76. Biron, I., *Émaux sur Métal – du IXe au XIXe Siècle. Histoire, Technique et Matériaux*. 2015: Faton edition.
77. Sterpenich, J. and G. Libourel, *Using stained glass windows to understand the durability of toxic waste matrices*. Chemical Geology, 2001. **174**: p. 181-193.
78. France Commissariat à l'énergie, a., V. Centre de, and I.I.S.e.t.d.L. Université Montpellier, *Actes des journées sur le Verre: Université d'été CEA/VALRHÔ = CEA/VALRHÔ Summer Session proceedings Glass ; Recherche scientifique pour un confinement de haute performance = Scientific research for high performance containment, 31 août-7 septembre 1997 = 31 august-7 september 1997, Méja*. Commissariat à l'énergie atomique 1997.
79. Sterpenich, J., *Altération des vitraux médiévaux - Contribution à l'étude du comportement à long terme des verres de confinement*. 1998, Université Henri Poincaré. p. 440.
80. Barger, M.S., D.K. Smith, and W.B. White, *Characterization of corrosion products on old protective glass, especially daguerreotype cover glasses*. Journal of Materials Science, 1989. **24**(4): p. 1343-1356.
81. Rebiscoul, D., et al., *Protective properties and dissolution ability of the gel formed during nuclear glass alteration*. Journal of Nuclear Materials, 2005. **342**(1): p. 26-34.
82. Rebiscoul, D., et al., *Morphological evolution of alteration layers formed during nuclear glass alteration: new evidence of a gel as a diffusive barrier*. Journal of Nuclear Materials, 2004. **326**(1): p. 9-18.
83. Cailleteau, C., et al., *Why Do Certain Glasses with a High Dissolution Rate Undergo a Low Degree of Corrosion?* The Journal of Physical Chemistry C, 2011. **115**(13): p. 5846-5855.
84. Le Guillou, C., et al., *New experimental approach to study aqueous alteration of amorphous silicates at low reaction rates*. Chemical Geology, 2015. **412**: p. 179-192.
85. Balasubramanian, R., et al., *Investigation of the vaporization of boric acid by transpiration thermogravimetry and knudsen effusion mass spectrometry*. J. Phys. Chem. B, 2008. **112**: p. 13873-13884.
86. Gaillardet, J., et al., *Evaporation and Sublimation of Boric Acid: Application for Boron Purification from Organic Rich Solutions*. Geostandards Newsletter, 2001. **25**(1): p. 67-75.
87. Siboni, S. and C. Della Volpe, *Some mathematical aspects of the Kelvin equation*. Computers & Mathematics with Applications, 2008. **55**(1): p. 51-65.
88. Sicard, L., et al., *Study of the kinetics of glass alteration by small-angle X-ray scattering*. Journal of Physical Chemistry B, 2004. **108**: p. 7702-7708.

89. Girard, L., M. Arab, and O. Spalla, *Time resolved alteration process of oxide glasses*. Journal of Colloid and Interface Science, 2008. **319**(1): p. 214-225.
90. Toquer, G., et al., *Effect of leaching concentration and time on the morphology of pores in porous glasses*. Journal of Non-Crystalline Solids, 2011. **357**(6): p. 1552-1557.
91. Kanehashi, K., *Structural roles of calcium in alkaline and alkaline-earth aluminosilicate glasses by solid-state ^{43}Ca , ^{17}O and ^{27}Al NMR*. Solid State Nuclear Magnetic Resonance, 2017. **84**: p. 158-163.
92. Guo, R., et al., *The effect of magnesium on the local structure and initial dissolution rate of simplified UK Magnox waste glasses*. Journal of Non-Crystalline Solids, 2018. **497**: p. 82-92.
93. Angeli, F., et al., *Influence of glass composition and alteration solution on leached silicate glass structure : a solid-state NMR investigation*. Geochimica et Cosmochimica Acta, 2006. **70**(10): p. 2577-2590.
94. Thien, B., et al., *Structural identification of a trioctahedral smectite formed by the aqueous alteration of a nuclear glass*. Applied Clay Science, 2010. **49**: p. 135-141.
95. Sicard, L., et al., *Dissolution of Oxide Glasses: A Process Driven by Surface Generation*. The Journal of Physical Chemistry C, 2008. **112**(5): p. 1594-1603.
96. Pons-Corbeau, J., et al., *Quantitative Surface Analysis by Glow Discharge Optical Spectrometry*. Surface and interface analysis, 1986. **9**: p. 21-25.

Tables and figures

List of Figures

Figure 1 (a) SEM image (cross-section) of AVM6 (altered for 180 days at 50°C and 95%RH) showing an irregularly altered zone; (b) TEM image of AVM6 (cross-section) (altered for 557 days) showing a porous irregularly altered zone on the left side of the image and an unaltered zone adjacent to it. (from top) the resin, the layer of phyllosilicates of approx. 200-250 nm thickness, a homogeneous gel layer of approx. 70 nm thickness and the very porous altered zone. The pores visible beneath the homogeneous gel layer on the right side of the image were enlarged due to exposure to electron beam; but this clearly shows the presence of the homogeneous gel layer even in zones where irregular altered zone is not present; (c) SEM image of AVM10 (cross-section) (altered for 180 days) showing an irregularly altered zone; (d) STEM-BF image of AVM10 (cross-section) (altered for 557 days). This micro-section shows one irregularly altered zone spanning approx. 230 nm and the presence of a uniform approx. 30 nm thick gel layer throughout the micro-section 36

Figure 2 (a) SEM image of AVM6 (altered for 180 days at 50°C and 95% RH) showing leafy precipitates and needle shaped crystalline phases; (b) TEM image of AVM6 (cross-section) (altered for 180 days) showing a 70 nm thick layer of phyllosilicates above an approx. 50 nm thick homogeneous gel layer. The porous irregularly altered zone is present beneath the homogeneous gel layer; (c) SEM image of AVM6 (altered for 557 days) - Formation of crystalline precipitates along straight lines assumed to be surface defects created while polishing; (d) Closer look at image (c) – Cluster of needle shape precipitates; (e) TEM image of AVM10 (cross-section) (altered for 180 days) - The image shows the presence of poorly crystallized phyllosilicates of approx. 330 nm thickness at the surface; the black circular spots are

1074	precipitates rich in Ag, Mo and P. Beneath the precipitates, a uniform gel layer of 15-30 nm is present. A	
1075	very porous altered zone is present beneath the homogeneous gel layer; (f) TEM image of AVM10 (cross-	
1076	section) (altered for 557 days) – The image shows the presence of well-developed approx. 70 nm thick	
1077	phyllosilicate layer containing precipitates rich in Ag, Mo and P (circular spots). Underneath, an approx.	
1078	27 nm thick uniform gel layer is present. The porosity visible at the gel-glass interface is an artificial	
1079	enlargement of pores due to exposure to electron beam.....	37
1080	Figure 3 (a) SEM image of QMg (altered for 180 days at 50°C and 95% RH) showing a carpet of thread-like	
1081	precipitate and fibrous cluster of secondary precipitates; (b) SEM image of QMg (altered for 557 days)	
1082	showing a gnawed appearance at the altered sample surface; (c) SEM image of AVMV4 (altered for 180	
1083	days) showing a similar altered surface to QMg altered for the same duration; (d) SEM image of AVMV4	
1084	(altered for 557 days) showing holes/pits of size 400-500 nm; (e) TEM image of AVMV4-557 (cross-	
1085	section) showing a layer of phyllosilicates of varying thickness on altered glass surface and a uniform	
1086	homogeneous gel layer of approx. 80 nm thickness; (f) A zoom of image (e), showing the homogeneous	
1087	gel layer with a mixture of amorphous and crystalline precipitates on the altered surface. There appear	
1088	to be more crystallized precipitates towards the surface and at the interface of gel-layer precipitate-layer	
1089	38
1090	Figure 4 (a) STEM image of QMg (cross-section) (altered for 180 days at 50°C and 95% RH); (b) TEM	
1091	image of Q (cross-section) (altered for 180 days)	39
1092	Figure 5 (a) TEM image of QCa (cross-section) altered for 180 days at 50°C and 95% RH; (b) SEM image of	
1093	QCa altered for 557 days at 50°C and 95% RH; (c) SEM image of cross-section of QCa altered for 557 days	
1094	39
1095	Figure 6 ToF-SIMS profiles of all six glasses altered at 50°C and 95% RH for 180 days; The profiles of only	
1096	the major elements of the AVM glasses are shown here	40
1097	Figure 7 SAXS spectra of the glasses (a) Q and (b) QCa that were unaltered (black squares), altered for	
1098	180 days (blue circles) and 557 days (orange triangles); The red dotted lines represent $I \propto q^{-4}$; The inset	
1099	graphs show the plot of $(I(\text{corr}) * q^4)$ vs. q highlighting the shift of the porod regime towards lower q with	
1100	increasing duration of alteration; $I(\text{corr})$ is a result of data treatment to separate the intensity scattered	
1101	by grain envelopes and the inner pores of the gel layer	41
1102	Figure 8 Evolution of $(A-A_0)$ with time; (i. e.) The increase in the absorbance of the SiOH band at 3600 cm^{-1}	
1103	of deconvoluted FTIR spectra of glasses altered at 50°C and 95% RH until 557 days (A) with respect to	
1104	the absorbance of the SiOH band of the deconvoluted FTIR spectrum of the unaltered glass monolith	
1105	(A_0) . (a) Evolution of $(A-A_0)$ for all six glasses; (b) Evolution of $(A-A_0)$ of the glasses Q and QCa; (c)	
1106	Evolution of $(A-A_0)$ of the glasses AVMV4 and QMg; (d) A zoom of image (a) to observe closely the	
1107	evolution of $(A-A_0)$ of AVM10 glass until 180 days.....	42
1108	Figure 9 (a) Description of the altered layer morphology of the six glasses that were vapor hydrated at	
1109	50°C and 95%RH for 180 days and 557 days; This description was constructed based on TEM images and	
1110	ToF-SIMS profiles at 557 days; X-axis is the mol% of elements (without considering O) calculated from	
1111	ToF-SIMS intensities based on Pons-Corbeau method ([96]); y-axis is the distance from the surface in nm;	
1112	The portions of the ToF-SIMS profiles that correspond to pristine glass, homogeneous gel layer and	
1113	smectites were chosen approximatively by a combined analysis of TEM images and ToF-SIMS profiles; (b)	
1114	Schematic description of the morphology of the altered glasses	43
1115		

List of tables

Table 1 Glass compositions (mol% of oxides) (measured by ICP) (error 3%) and fraction of Non-Bridging Oxygen atoms (NBO) and percent of boron in 4-coordination (^{IV} B) (error 3-8%).....	44
Table 2 Composition (normalized to 4 moles of Si) of phyllosilicates measured by STEM-EDX analyses (at least 12% relative error).....	45
Table 3 Thickness (in nm) of the altered layer (altered at 50°C and 95% RH for 180 days and 557 days each); (ToF-SIMS) is measured from equation 2.4.4.2; (TEM) is measured based on the density difference between pristine glass and gel layer in TEM images	45
Table 4 Porosity, pore-size and surface area of gel calculated from SAXS data; ϕ_{gel} corresponds to the volume fraction of gel calculated from ToF-SIMS profiles of monoliths that were used to calculate the porosity of the gel formed on glass powders.....	46

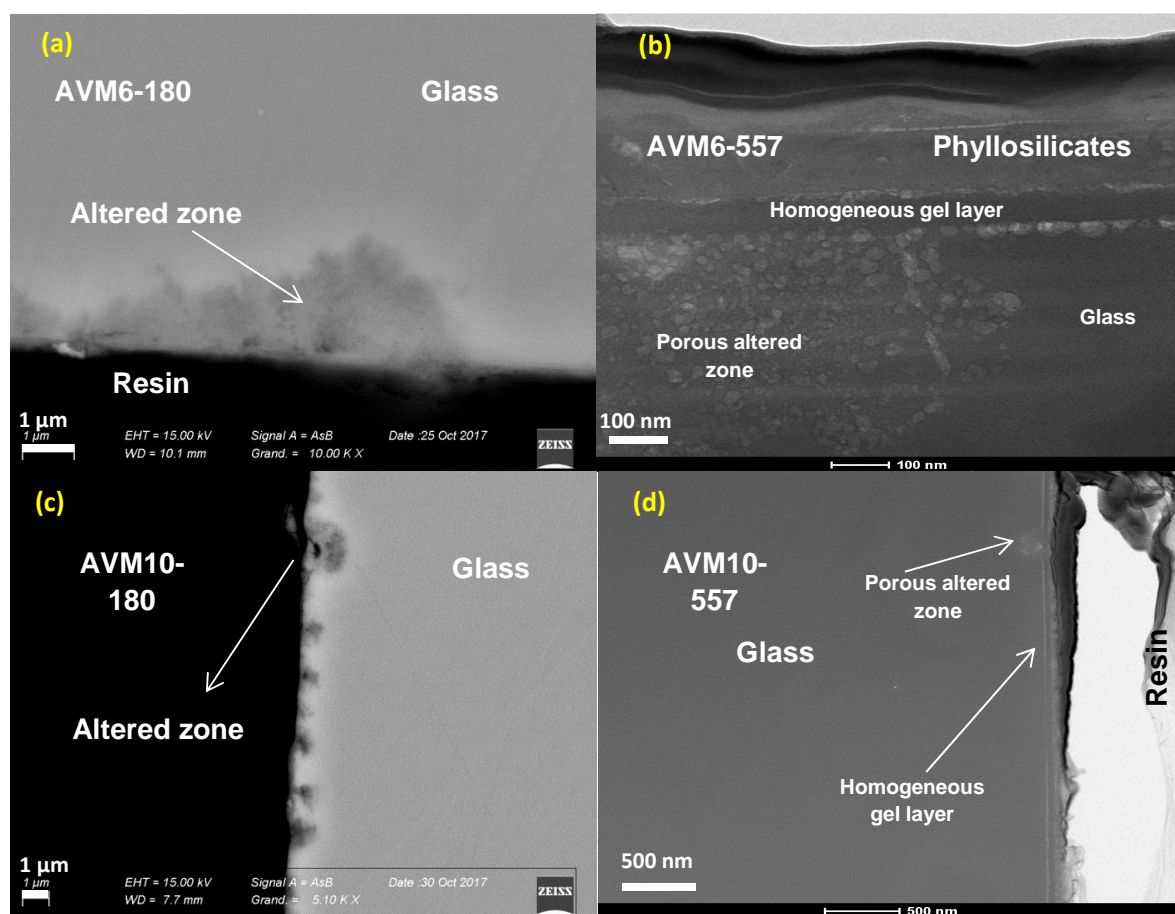


Figure 1 (a) SEM image (cross-section) of AVM6 (altered for 180 days at 50°C and 95%RH) showing an irregularly altered zone; (b) TEM image of AVM6 (cross-section) (altered for 557 days) showing a porous irregularly altered zone on the left side of the image and an unaltered zone adjacent to it. (from top) the resin, the layer of phyllosilicates of approx. 200-250 nm thickness, a homogeneous gel layer of approx. 70 nm thickness and the very porous altered zone. The pores visible beneath the homogeneous gel layer on the right side of the image were enlarged due to exposure to electron beam; but this clearly shows the presence of the homogeneous gel layer even in zones where irregular altered zone is not present; (c) SEM image of AVM10 (cross-section) (altered for 180 days) showing an irregularly altered zone; (d) STEM-BF image of AVM10 (cross-section) (altered for 557 days). This micro-section shows one irregularly altered zone spanning approx. 230 nm and the presence of a uniform approx. 30 nm thick gel layer throughout the micro-section

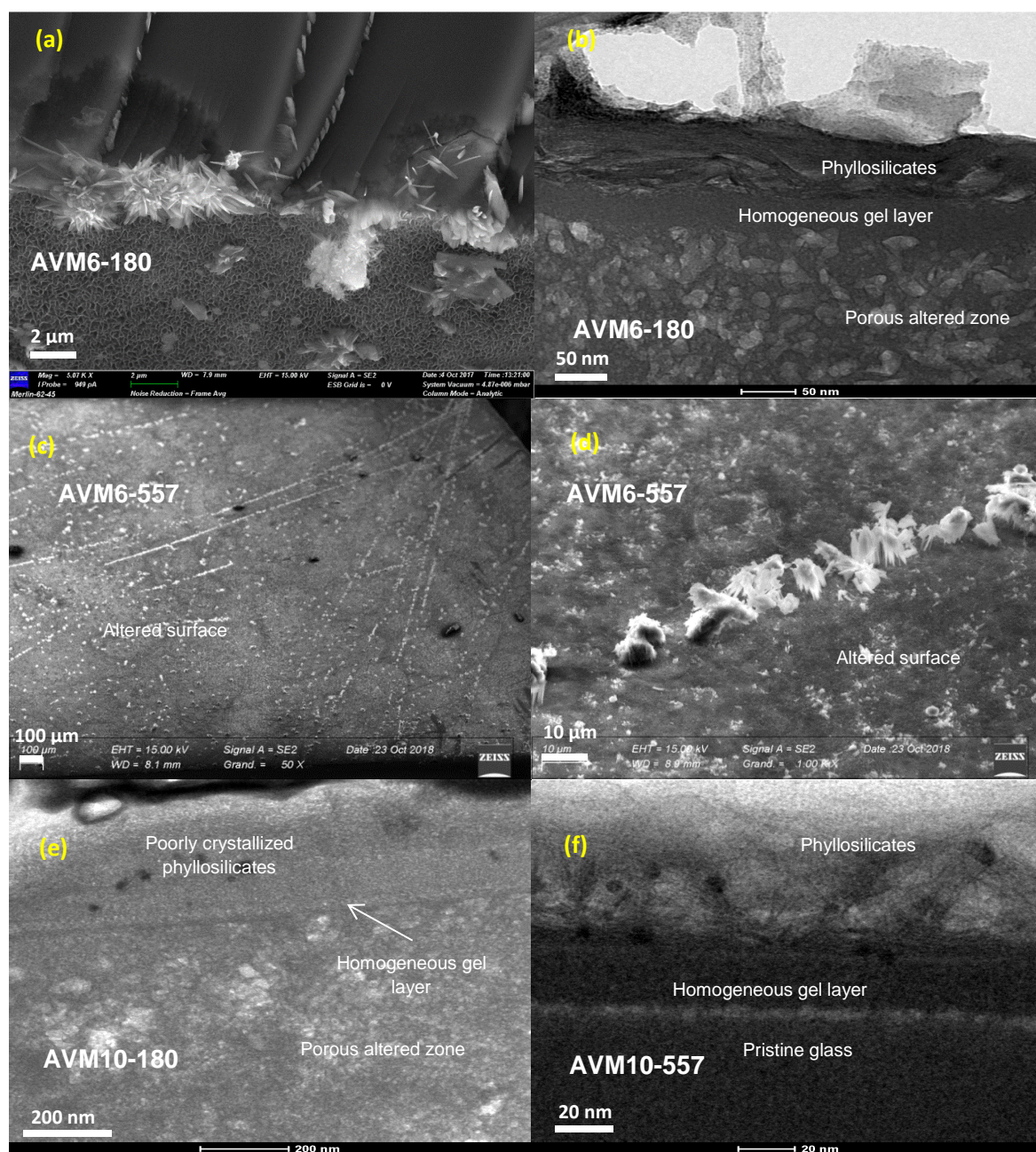


Figure 2 (a) SEM image of AVM6 (altered for 180 days at 50°C and 95% RH) showing leafy precipitates and needle shaped crystalline phases; (b) TEM image of AVM6 (cross-section) (altered for 180 days) showing a 70 nm thick layer of phyllosilicates above an approx. 50 nm thick homogeneous gel layer. The porous irregularly altered zone is present beneath the homogeneous gel layer; (c) SEM image of AVM6 (altered for 557 days) - Formation of crystalline precipitates along straight lines assumed to be surface defects created while polishing; (d) Closer look at image (c) - Cluster of needle shape precipitates; (e) TEM image of AVM10 (cross-section) (altered for 180 days) - The image shows the presence of poorly crystallized phyllosilicates of approx. 330 nm thickness at the surface; the black circular spots are precipitates rich in Ag, Mo and P. Beneath the precipitates, a uniform gel layer of 15-30 nm is present. A very porous altered zone is present beneath the homogeneous gel layer; (f) TEM image of AVM10 (cross-section) (altered for 557 days) - The image shows the presence of well-developed approx. 70 nm thick phyllosilicate layer containing precipitates rich in Ag, Mo and P (circular spots). Underneath, an approx. 27 nm thick uniform gel layer is present. The porosity visible at the gel-glass interface is an artificial enlargement of pores due to exposure to electron beam.

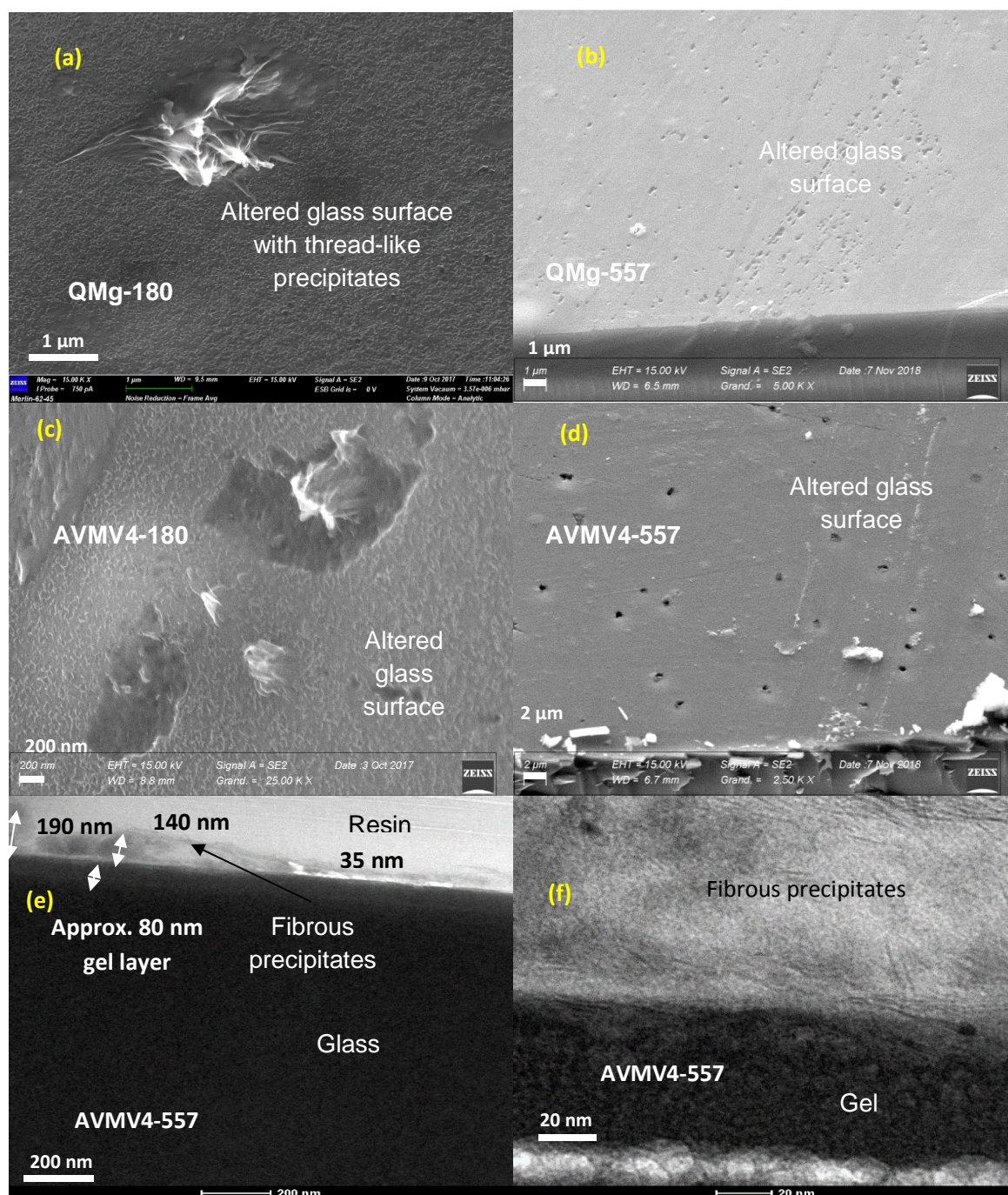


Figure 3 (a) SEM image of QMg (altered for 180 days at 50°C and 95% RH) showing a carpet of thread-like precipitate and fibrous cluster of secondary precipitates; (b) SEM image of QMg (altered for 557 days) showing a gnawed appearance at the altered sample surface; (c) SEM image of AVMV4 (altered for 180 days) showing a similar altered surface to QMg altered for the same duration; (d) SEM image of AVMV4 (altered for 557 days) showing holes/pits of size 400-500 nm; (e) TEM image of AVMV4-557 (cross-section) showing a layer of phyllosilicates of varying thickness on altered glass surface and a uniform homogeneous gel layer of approx. 80 nm thickness; (f) A zoom of image (e), showing the homogeneous gel layer with a mixture of amorphous and crystalline precipitates on the altered surface. There appear to be more crystallized precipitates towards the surface and at the interface of gel-layer precipitate-layer

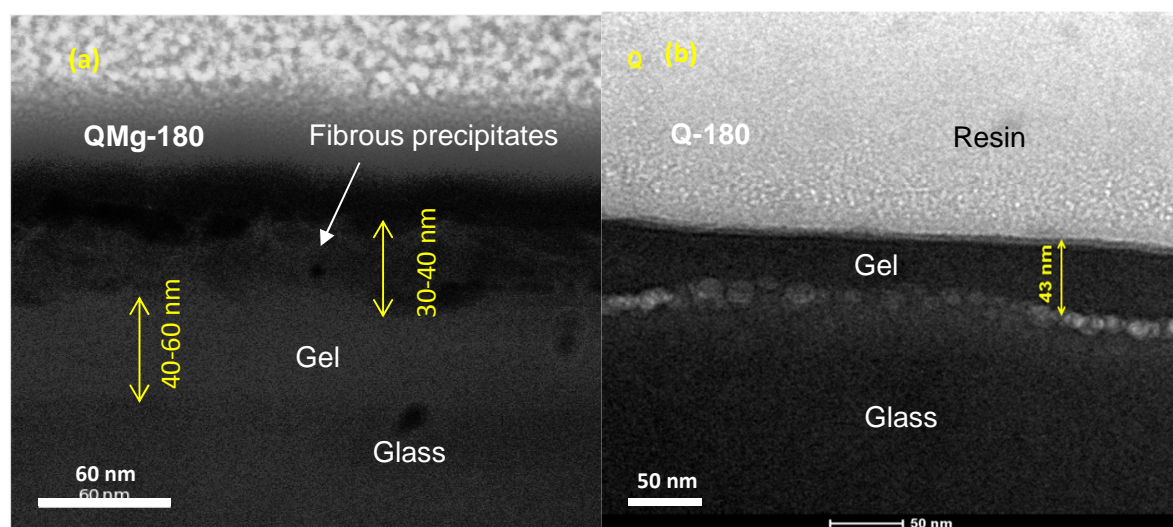


Figure 4 (a) STEM image of QMg (cross-section) (altered for 180 days at 50°C and 95% RH); (b) TEM image of Q (cross-section) (altered for 180 days)

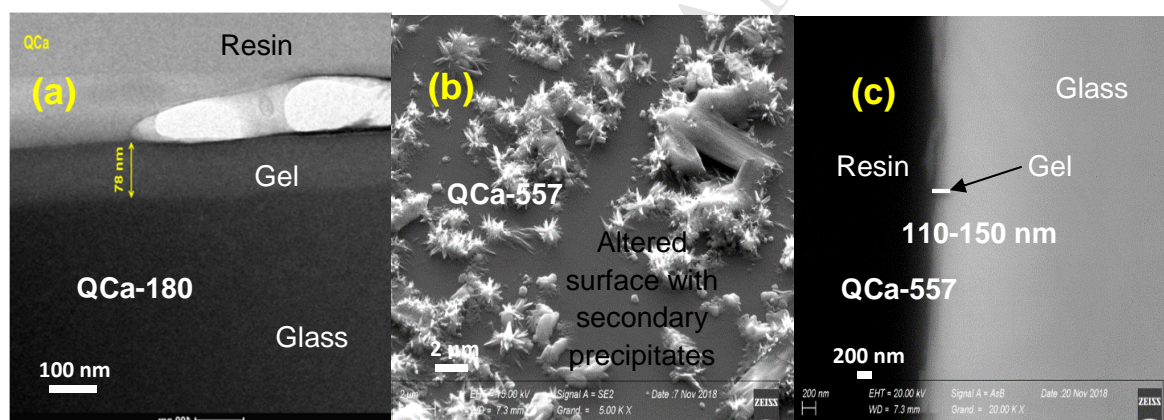


Figure 5 (a) TEM image of QCa (cross-section) altered for 180 days at 50°C and 95% RH; (b) SEM image of QCa altered for 557 days at 50°C and 95% RH; (c) SEM image of cross-section of QCa altered for 557 days

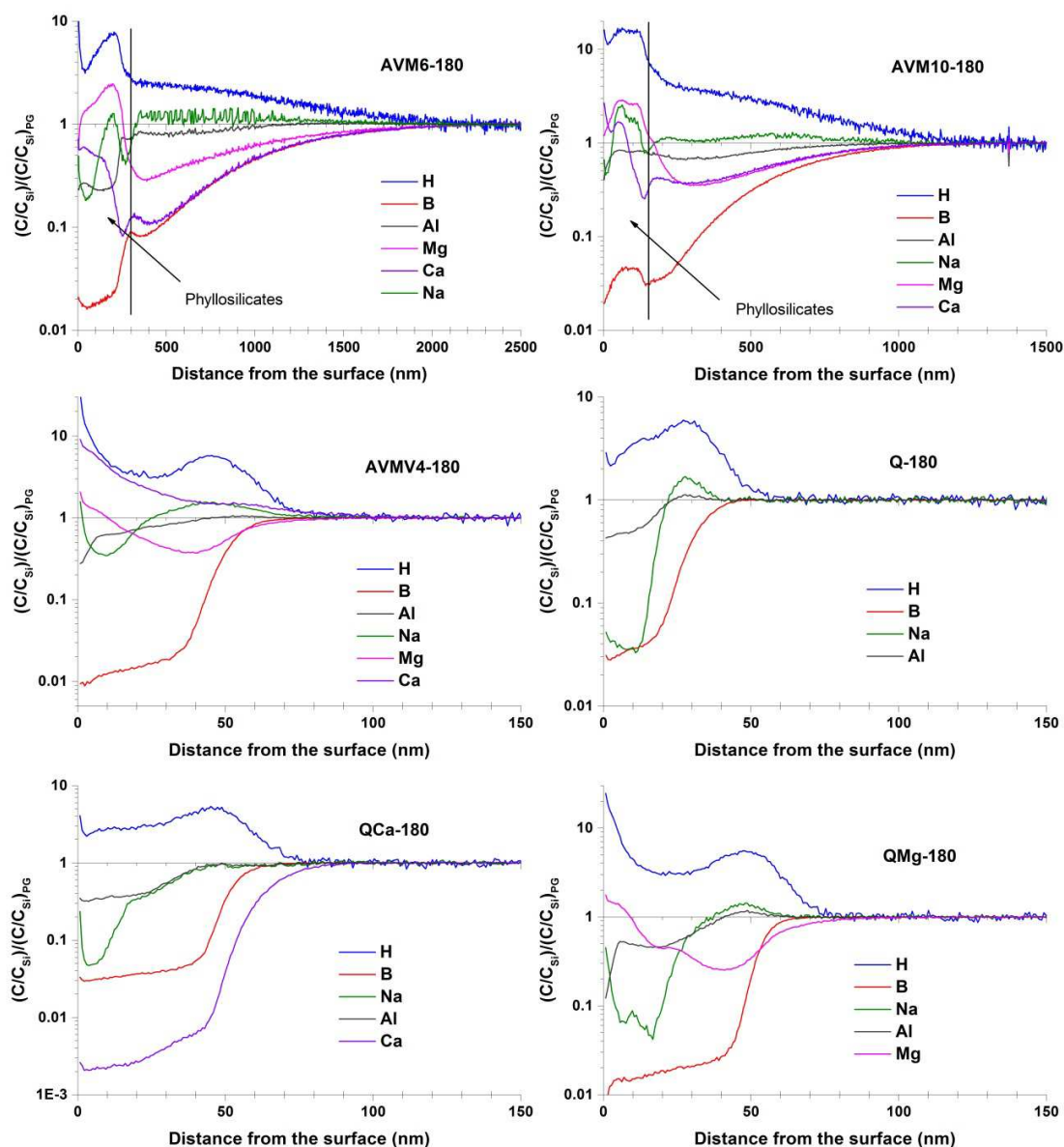


Figure 6 ToF-SIMS profiles of all six glasses altered at 50°C and 95% RH for 180 days; The profiles of only the major elements of the AVM glasses are shown here

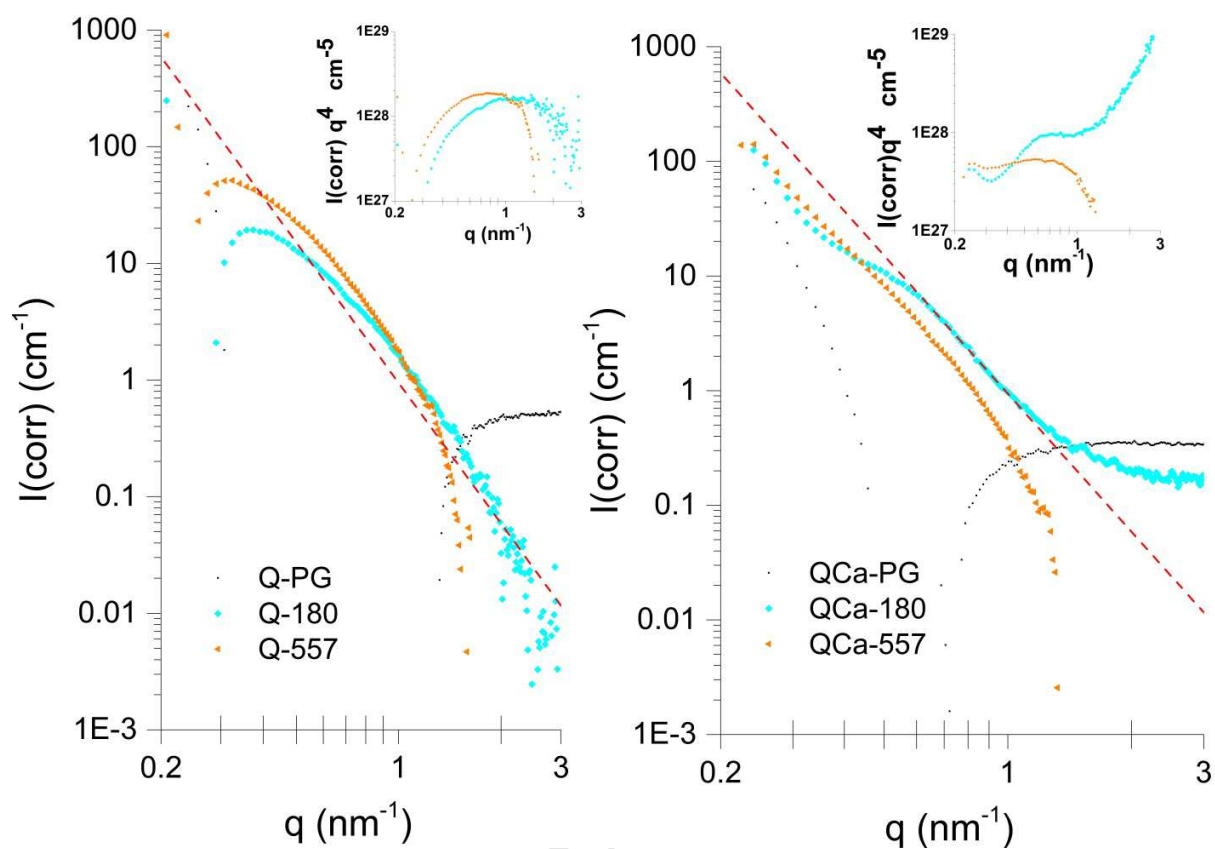


Figure 7 SAXS spectra of the glasses (a) Q and (b) QCa that were unaltered (black squares), altered for 180 days (blue circles) and 557 days (orange triangles); The red dotted lines represent $I \propto q^{-4}$; The inset graphs show the plot of $(I(\text{corr}) \cdot q^4)$ vs. q highlighting the shift of the porod regime towards lower q with increasing duration of alteration; $I(\text{corr})$ is a result of data treatment to separate the intensity scattered by grain envelopes and the inner pores of the gel layer

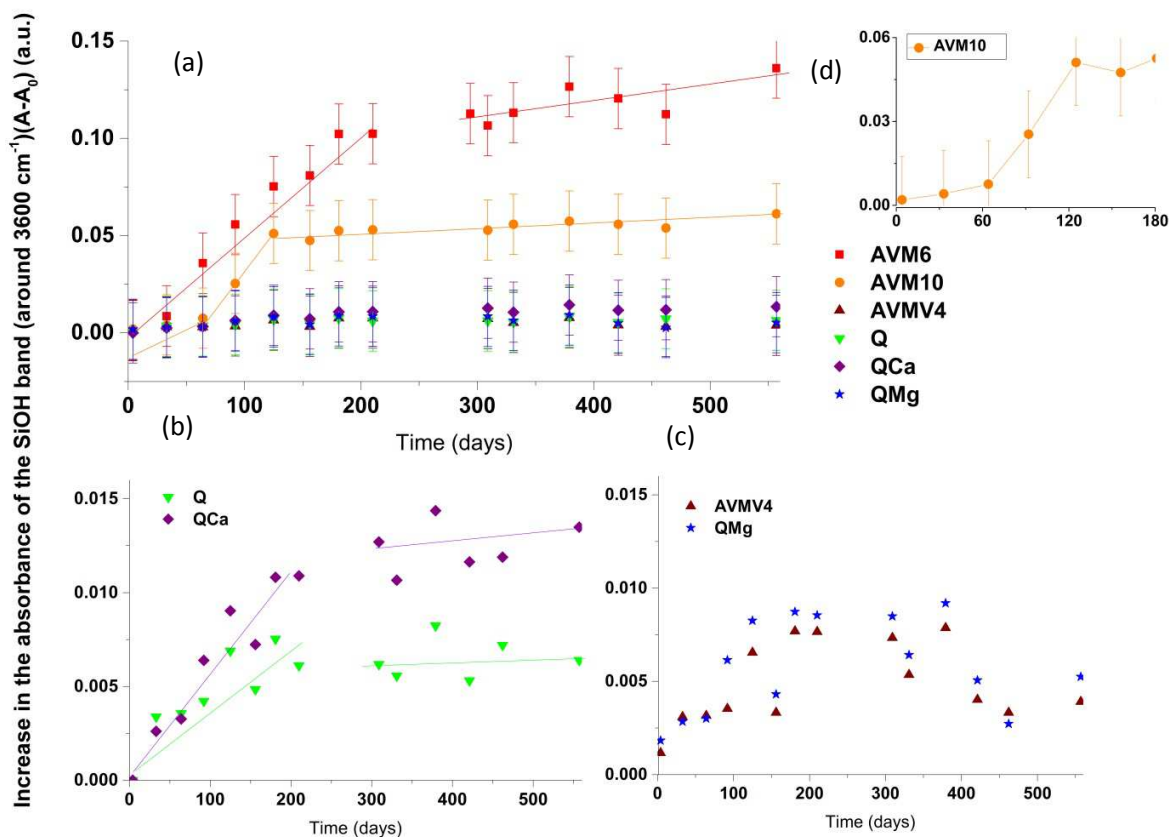


Figure 8 Evolution of $(A-A_0)$ with time; (i. e.) The increase in the absorbance of the SiOH band at 3600 cm⁻¹ of deconvoluted FTIR spectra of glasses altered at 50°C and 95% RH until 557 days (A) with respect to the absorbance of the SiOH band of the deconvoluted FTIR spectrum of the unaltered glass monolith (A_0). (a) Evolution of $(A-A_0)$ for all six glasses; (b) Evolution of $(A-A_0)$ of the glasses Q and QCa; (c) Evolution of $(A-A_0)$ of the glasses AVMV4 and QMg; (d) A zoom of image (a) to observe closely the evolution of $(A-A_0)$ of AVM10 glass until 180 days

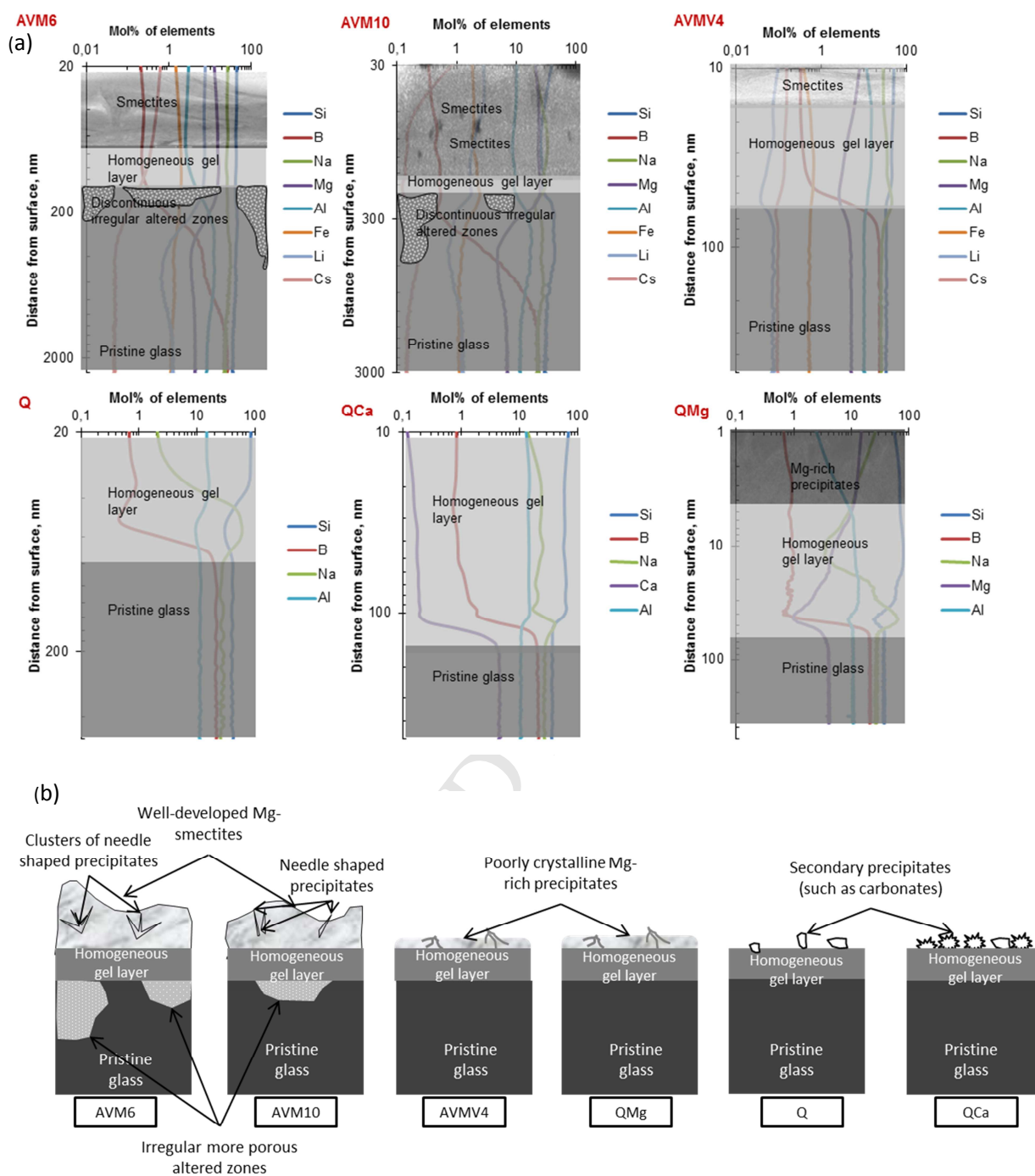


Figure 9 (a) Description of the altered layer morphology of the six glasses that were vapor hydrated at 50°C and 95%RH for 180 days and 557 days; This description was constructed based on TEM images and ToF-SIMS profiles at 557 days; X-axis is the mol% of elements (without considering O) calculated from ToF-SIMS intensities based on Pons-Corbeau method ([96]); y-axis is the distance from the surface in nm; The portions of the ToF-SIMS profiles that correspond to pristine glass, homogeneous gel layer and smectites were chosen approximatively by a combined analysis of TEM images and ToF-SIMS profiles; (b) Schematic description of the morphology of the altered glasses

1219

1220 *Table 1 Glass compositions (mol% of oxides) (measured by ICP) (error 3%) and fraction of Non-Bridging Oxygen*
 1221 *atoms (NBO) and percent of boron in 4-coordination (^{IV}B) (error 3-8%)*

	AVMV4	AVM6	AVM10	Q	QCa	QMg
SiO₂	48.16	49.29	43.39	57.48	52.67	52.6
Al₂O₃	7.15	5.88	8.30	8.07	7.49	7.74
B₂O₃	16.71	18.64	16.29	15.28	14.6	15.02
Na₂O	18.61	16.65	16.39	19.17	19.01	18.83
CaO	0.04	0.24	0.24	0	6.23	0
MgO	7.15	6.28	10.38	0	0	5.81
Li₂O	0.05	0.89	0.91	0	0	0
ZrO₂	0.22	0.10	0.29	0	0	0
Fe₂O₃	0.38	0.79	0.81	0	0	0
NiO	0.13	0.27	0.27	0	0	0
Cr₂O₃	0.09	0.20	0.20	0	0	0
P₂O₅	0.08	0.00	0.81	0	0	0
SrO	0.06	0.03	0.08	0	0	0
Y₂O₃	0.02	0.01	0.02	0	0	0
MoO₃	0.29	0.13	0.39	0	0	0
MnO	0.10	0.05	0.13	0	0	0
Ag₂O	0.02	0.01	0.03	0	0	0
CdO	0.05	0.26	0.26	0	0	0
TeO₂	0.03	0.01	0.03	0	0	0
Cs₂O	0.07	0.03	0.09	0	0	0
BaO	0.06	0.03	0.08	0	0	0
La₂O₃	0.05	0.02	0.06	0	0	0
Ce₂O₃	0.05	0.02	0.07	0	0	0
Pr₂O₃	0.02	0.01	0.03	0	0	0
Nd₂O₃	0.14	0.04	0.10	0	0	0
RuO₂	0.17	0.08	0.22	0	0	0
PdO	0.11	0.05	0.15	0	0	0
Fraction of NBO	0.134	0.158	0.162	0.036	0.111	0.115
Percent of ^{IV}B	39	20	27	48.5	46.5	37

1222

1223

1224

1225 *Table 2 Composition (normalized to 4 moles of Si) of phyllosilicates measured by STEM-EDX analyses (at least 12% relative error)*

	O	Mg	Al	Si	Ca	Cr	Fe	Nd
AVM6-180	13.60	1.51	0.18	4.00	0.07	0.01	0.18	0.01
AVM6-557	15.62	1.72	0.20	4.00	0.06	0.03	0.16	0.00

	O	Mg	Al	Si	P	Ca	Cr	Fe	Nd
AVM10-180	35.00	3.44	1.09	4.00	0.21	0.10	0.00	0.27	0.08
AVM10-557	20.82	2.01	1.06	4.00	0.17	0.16	0.01	0.23	0.00

1226
1227 *Table 3 Thickness (in nm) of the altered layer (altered at 50°C and 95% RH for 180 days and 557 days each); (ToF-SIMS) is*
1228 *measured from equation 2.4.4.2; (TEM) is measured based on the density difference between pristine glass and gel layer in TEM*
1229 *images*

Duration of alteration	180 days		557 days	
	(ToF-SIMS)	(TEM)	(ToF-SIMS)	(TEM)
AVM6	1060	(70 nm homogeneous layer + Irregular alteration + surface precipitates)	900	(70 nm homogeneous layer + Irregular alteration + surface precipitates)
AVM10	630	(~30 nm homogeneous layer + Irregular alteration + surface precipitates)	905	(~30 nm homogeneous layer + Irregular alteration + surface precipitates)
AVMV4	52	-	64	(~80 nm homogeneous altered layer + surface precipitates)
Q	31	~43 nm homogeneous altered layer	66	~76 nm homogeneous altered layer
QCa	52	~78 nm homogeneous altered layer	121	110-150 nm homogeneous altered layer (SEM)
QMg	53	(~60 nm altered layer + ~30 nm fibrous precipitates)	66	(~76 nm homogeneous altered layer + surface precipitates)

Table 4 Porosity, pore-size and surface area of gel calculated from SAXS data; ϕ_{gel} corresponds to the volume fraction of gel calculated from ToF-SIMS profiles of monoliths that were used to calculate the porosity of the gel formed on glass powders

	Time (days)	Porosity (%)	pore diameter, nm	Surface area of pores, m ² /g	ϕ_{gel}
Q	180	65	4.3	451	0.05
	557	44	5	264	0.1
QCa	180	27	5.1	158	0.08
	557	9	7.5	37.6	0.19
AVM6	11	66	4.4	328	0.06
	31	47	4.5	235	0.15
	90	11	4.8	58.2	0.64

Highlights

- Rate-controlling vapor hydration mechanism is dependent on glass composition
- The molar ratio of $\text{Al}_2\text{O}_3/\text{MgO}$ affects glass alteration kinetics in vapor phase
- $(\text{Al}_2\text{O}_3/\text{MgO}) < 1$ seems to result in significant precipitation of Mg-smectites
- Difference between relative glass durability in aqueous medium and vapor phase
- Porosity and pore-size of altered layer is similar in the two alteration media